catalysts

MDPI

Review

Recent Progress in Plasmonic Hybrid Photocatalysis for CO_2 Photoreduction and C–C Coupling Reactions

Hyeon Ho Shin [1,2], Yung Doug Suh [2,3,*] and Dong-Kwon Lim [1,*]

[1] KU-KIST Graduate School of Converging Science and Technology, Korea University, 145 Anam-ro, Seongbuk-gu, Seoul 02841, Korea; sinhh10@gmail.com
[2] Laboratory for Advanced Molecular Probing, Eco-Friendly New Materials Research Center, Korea Research Institute of Chemical Technology, 141 Gajeong-ro, Yuseong-gu, Daejeon 34114, Korea
[3] School of Chemical Engineering, Sungkyunkwan University (SKKU), Suwon 440-746, Korea
* Correspondence: ydsuh@krict.re.kr (Y.D.S.); dklim@korea.ac.kr (D.-K.L.); Tel.: +82-42-860-7597 (Y.D.S.); +82-2-3290-4611 (D.-K.L.)

Abstract: Plasmonic hybrid nanostructures have been investigated as attractive heterogeneous photocatalysts that can utilize sunlight to produce valuable chemicals. In particular, the efficient photoconversion of CO_2 into a stable hydrocarbon with sunlight can be a promising strategy to achieve a sustainable human life on Earth. The next step for hydrocarbons once obtained from CO_2 is the carbon–carbon coupling reactions to produce a valuable chemical for energy storage or fine chemicals. For these purposes, plasmonic nanomaterials have been widely investigated as a visible-light-induced photocatalyst to achieve increased efficiency of photochemical reactions with sunlight. In this review, we discuss recent achievements involving plasmonic hybrid photocatalysts that have been investigated for CO and CO_2 photoreductions to form multi-carbon products and for C–C coupling reactions, such as the Suzuki–Miyaura coupling reactions.

Keywords: plasmonic nano-catalysts; photocatalytic reaction; CO_2 reductions; C–C cross-coupling

check for updates

Citation: Shin, H.H.; Suh, Y.D.; Lim, D.-K. Recent Progress in Plasmonic Hybrid Photocatalysis for CO_2 Photoreduction and C–C Coupling Reactions. *Catalysts* **2021**, *11*, 155. https://doi.org/10.3390/catal11020155

Received: 18 December 2020
Accepted: 15 January 2021
Published: 22 January 2021

1. Introduction

Global population growth and industrial development have been continuously causing the consumption of fossil fuels, resulting in environmental pollution and energy shortages. Among various alternative energy sources, sun light is an eco-friendly, clean, and sustainable energy source that can produce more than tens of thousands of terawatts from the Earth's surface [1,2]. The sun light can be utilized in various ways in producing electricity, photochemical synthesis in plants, and a giant heat source to maintain biological systems on Earth [3–7]. Therefore, utilizing sun light as an energy source has been an attractive research topic in chemistry and materials sciences. Among many applications with light, mimicking the photosynthetic system with a catalyst and sun light will be greatly attracting and challenging areas.

In this regard, the efficient conversion of CO_2 into hydrocarbon with sun light is one plausible way to reduce the amount of CO_2 at atmosphere by producing stable chemicals, which can be utilized as an energy source when necessary [8,9]. To achieve this challenging goal, the first step is an efficient conversion of CO_2 into hydrocarbon, either C_1 or C_2. The next step is carbon–carbon coupling to produce multi-carbon products. Although these two types of reactions have different aspects, the reactions have the commonality of not only forming carbon-to-carbon bonds, but also their utility in the production of materials that can be used in other fields.

The first developed method for CO_2 conversion is the electrochemical approach, traced back to the 19th century [10]. The electrochemical method has the advantages of flexibility in the design of devices and individual optimization of components, but still has the disadvantage of requiring external energy (electricity). Subsequently, the photocatalytic approach was proposed, which was traced back to the 1970s [11–14]. Inspired by photosynthesis, solar-driven reduction of CO_2 has been considered as one of several possible solutions because it is renewable and eco-friendly energy that can reduce CO_2 concentration [12,15–17]. The general concept of a CO_2 reduction process in the photocatalytic system is shown in Figure 1a.

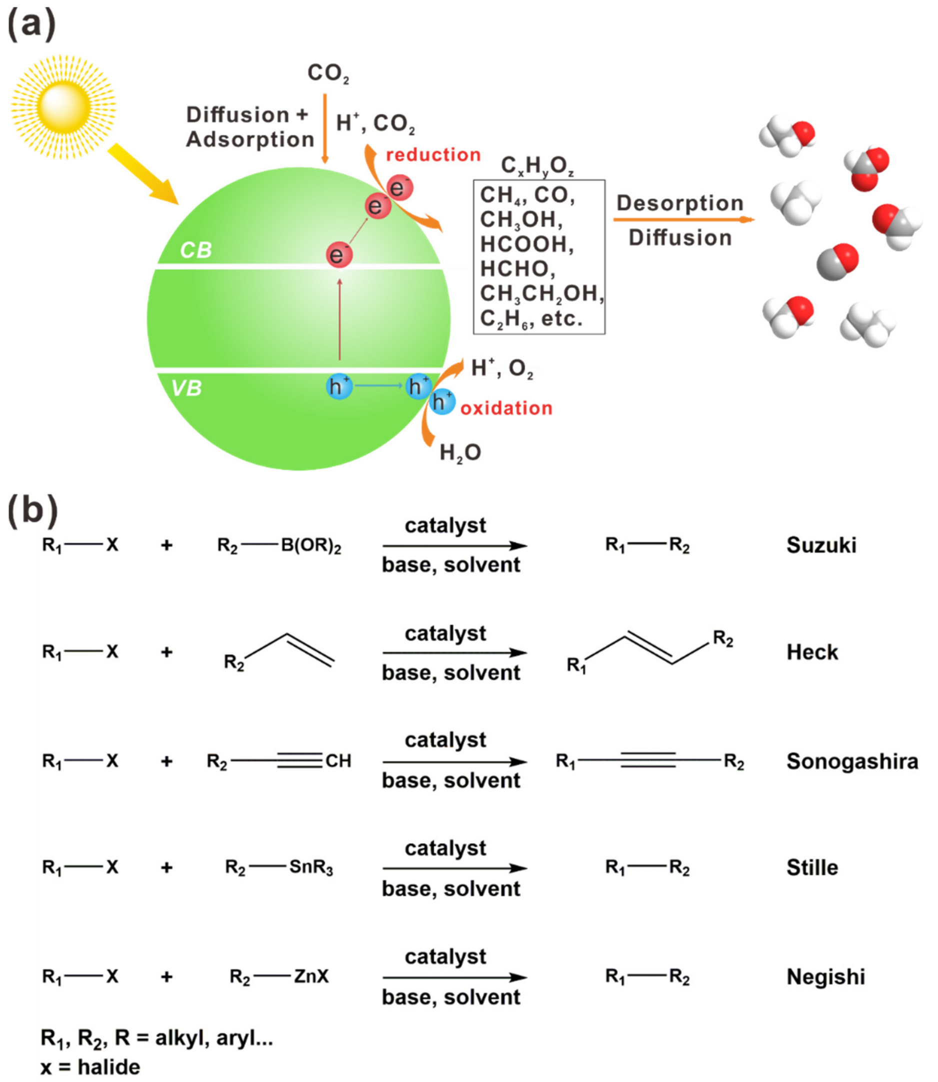

Figure 1. The carbon–carbon coupling reactions. (**a**) The general process of CO_2 reduction in a photocatalytic system inspired by photosynthesis and (**b**) the summary of carbon–carbon cross-coupling in organic chemistry.

The conversion of CO_2 into C_2 hydrocarbon is one type of a C–C coupling reaction [9,18]. However, the reaction requires a multi-step reaction involving multiple electrons. It is more difficult to conduct than the simple CO_2 conversion reaction. Therefore, the understanding and development of suitable catalysts, reaction conditions, etc. are essentially required to improve the efficiency of CO_2 conversion to multi-carbon products.

Carbon–carbon cross-couplings and related reactions, which are the other types of C–C coupling, present an important research direction in the field of chemistry [19–23]. After the reports of C–C coupling reactions in the 1970s [24–27], the reactions have been regarded as very powerful methods for forming C–C and C–heteroatom bonds. In recognition of their developments and applications conducted in the 1990s [28–31], in 2010, R. F. Heck, E.-I. Negishi, and A. Suzuki were awarded the Nobel Prize in Chemistry [32]. Even now, studies including the development of catalysts and reaction conditions are being extensively conducted to increase the efficiency of several named reactions, called Suzuki–Miyaura, Heck, Sonogashira, Stille, and Negishi, which are summarized in Figure 1b. The widely accepted mechanism of C–C cross-coupling reactions, including the Suzuki–Miyaura coupling, consists of three steps: (1) the oxidative addition of a catalyst such as palladium to the halide, which is the rate-determining step in most cases, (2) transmetalation, which is an organometallic reaction where the ligands are transferred from one species to the metal (II) complex, (3) the reductive elimination of corresponding products, and the restoration of the palladium catalyst [33]. Sufficient energy and specific reaction conditions are required to overcome the activation energy barrier, transfer the electrons, and make the reaction proceed [32,34,35]. These problems have led to a demand for sustainable, safe, and environmentally-friendly sources, such as solar energy.

Materials that are responsive to sunlight include plasmonic nanomaterials, semiconductors, and photosensitizers. When light is irradiated on the materials, electrons or energies are excited, causing chemical reactions and the transformation of solar energy into chemical energy. Accordingly, it is important to select the appropriate materials that can improve the catalytic efficiency. In particular, visible/IR-light-responsive materials need to be used because the visible-to-IR light accounts for ca. 95% of the solar light, while the proportion of UV of solar light is only ca. 5% [36–40]. Among possible materials, plasmonic nanoparticles, such as Au, Ag, and Cu, show strong interactions with visible-light and localized electromagnetic field due to their localized surface plasmon resonances (LSPR) [41–43]. The collective oscillation of electrons by LSPR induces to yield energetic electrons, called hot electrons, which can help boost the chemical reactions [41,44,45]. The changes in the size, shape, and composition of plasmonic nanomaterials can cause interactions in the near-infrared (NIR) region [46–50]. However, the hybridization of plasmonic nanomaterials with other materials such as semiconductors is necessary because of the extremely short lifetime of the hot electrons (<100 fs) [51,52]. In this review, we focus on the recent development of plasmonic nanomaterial-based photocatalysts for CO_2 reduction and C–C coupling.

2. Plasmonic Hybrid Photocatalysts for CO_2 Reduction into Hydrocarbon with Multi-Carbon Products

The increased CO_2 emission is a global problem, which strongly required us to start the immediate reduction [53–55]. Accordingly, CO_2 conversion into stable chemicals can be one of the key solutions, which can both reduce the amount of CO_2 and produce sustainable energy sources [8,56–58]. However, CO_2 is one of the most thermodynamically stable molecules due to its strong C=O double bond, which has made it difficult for many researchers to convert CO_2 into other fuels [37,57,59–61]. Even producing multi-carbon products is significantly more difficult than producing single carbon products because greater energy and a complex multi-step, multi-electron transfer processes are required [8,9,60,62]. Nonetheless, the production of multi-carbon chemicals is more desirable because of their higher energy densities, broader applicability, and use as more convenient storages and transportations [9,13,60,63–65].

Typically, semiconductors have been used for CO_2 conversion as a photocatalyst, in which the electrons are mainly derived from the excitons of photo-induced semiconductors [13,57,66–68]. However, the use of the limited wavelength of light have brought about the introduction of plasmonic metal NPs [9,13,69–71]. In the following part, we will discuss the introduction of plasmonic hybrid nanomaterials as a photocatalyst to improve the efficiency of CO_2 reduction reactions.

2.1. Gold Nanoparticle (AuNP)-Assisted Plasmonic Photocatalysts for CO_2 Reduction to Multi-Carbon Products

The gold nanoparticle (AuNP) is one of the promising visible-light-responsive materials that exhibit strong LSPR phenomenon with visible light [72]. Many advantages of AuNPs, including stability, low toxicity, and optical properties, have led many researchers to use AuNPs as photocatalysts [72,73]. There have been attempts to use AuNPs together with other materials, such as carbon nanoparticles and reduced graphene oxide to convert CO_2 into formic acid, but not to produce multi-carbon products [69,74].

The formation of more valuable multi-carbon products requires multiple electron–hole pairs involved in CO_2 reduction [75]. To generate abundant charge carriers, Tu et al. introduced AuNPs, showing a strong LSPR effect, into a TiO_2 hollow shell, which were called Au@TiO_2 yolk–shell hollow spheres [76]. According to this report, bare TiO_2 reduced CO_2 to produce CH_4 (1.33 µmoL g^{-1} h^{-1}), but not C_2H_6, while the Au@TiO_2 yolk–shell generated both CH_4 and C_2H_6, indicating the significant role of AuNPs in enhancing the photocatalytic yield and the generation of multi-carbon species with rates of 2.52 µmoL g^{-1} h^{-1} to produce CH_4 and 1.67 µmoL g^{-1} h^{-1} to produce C_2H_6, respectively, accelerating multiple e^-/h^+ reactions [76].

Yu et al. investigated product selectivity tuned by a light excitation attribute, which is a type of plasmonic control with polyvinylpyrrolidone (PVP)-capped AuNPs (11.8 ± 2.3 nm) [77]. They determined that higher photon energies (shorter wavelength) and flux (light intensity) tend to produce C_2H_6 rather than CH_4, showing C_2H_6 selectivity (Figure 2) [77]. Specifically, CH_4 production rates increased proportionally at higher photon energies, that is, shorter excitation wavelengths, but C_2H_6 was produced only at higher photon energies at a fixed laser intensity of 150 mW·cm^{-2} (Figure 2b). In addition, CH_4 production rates increased almost linearly with increasing photon flux, i.e., light intensity (~0.5 NP^{-1} h^{-1} of turnover frequency (TOF) under 532 nm, >0.9 NP^{-1} h^{-1} of turnover frequency under 488 nm), irrespective of the wavelength of light, and C_2H_6 generation was observed only at 488 nm of wavelength and above 300 mW cm^{-2} (~0.6 NP^{-1} h^{-1} of TOF at 750 mW cm^{-2}), indicating the presence of a threshold intensity for C_2H_6 production (Figure 2c,d).

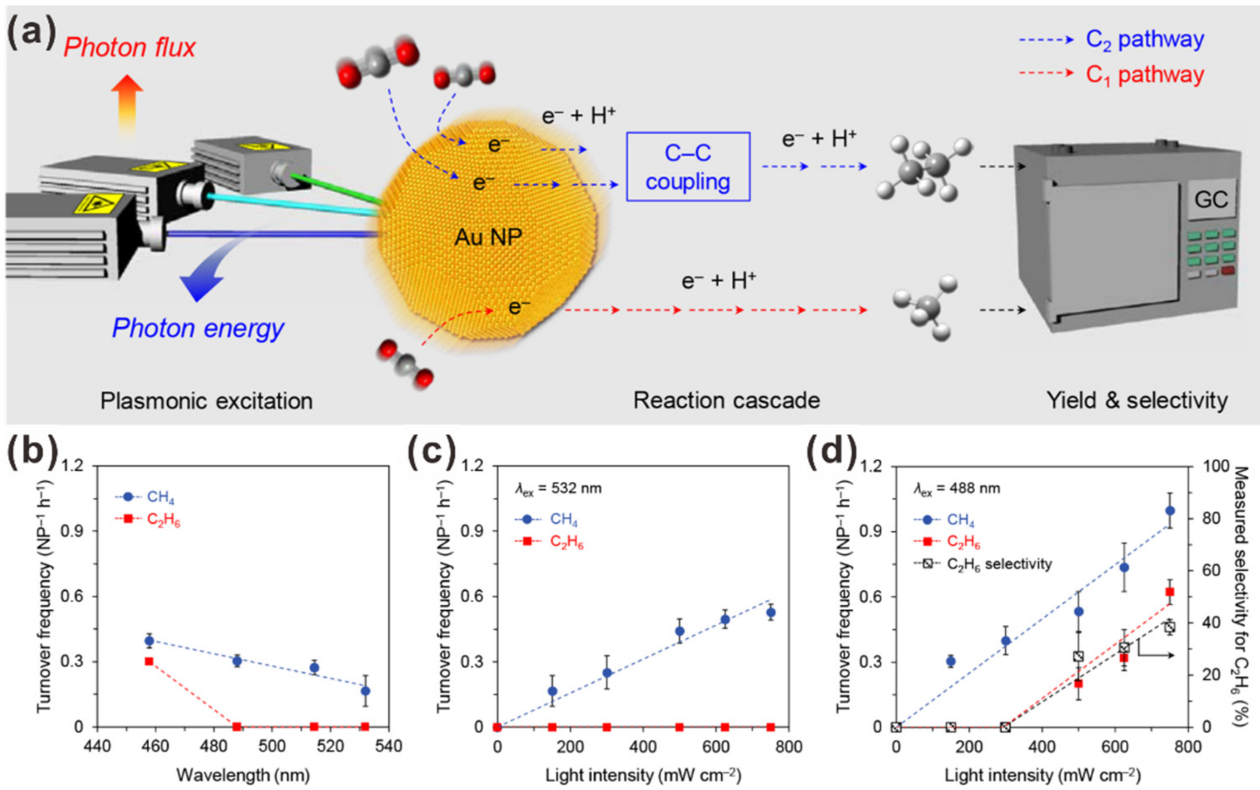

Figure 2. (**a**) The mechanism of CO_2 photoreduction into CH_4 and C_2H_6 with AuNPs (11.8 ± 2.3 nm), and the photocatalytic efficiency under (**b**) different wavelengths and (**c**,**d**) light intensities. Reproduced with permission from Reference [77]. Copyright 2018 American Chemical Society.

Zhao et al. also conducted plasmonic control of CO_2 conversion using metal/ZnO photocatalysts (Figure 3) [78]. They revealed that the production of higher levels of hydrocarbons, such as C_2H_6, is closely related to the coupling of the surface plasmon resonance (SPR) field with the intrinsic inner electric field, enabling the separation of electron–hole pairs and the polarization and activation of absorbed substrates. They found that Au interacts more strongly with semiconductors than Ag and Pd, which alters the molecular pathway of CO_2 conversion, resulting in a tremendous change in the selectivity of products by density functional theory (DFT) calculations, electron paramagnetic resonance spectroscopy, and Raman spectroscopy. By putting their results all together, they determined that only Au/ZnO can produce C_2H_6 with a rate of ~25 μmol g^{-1} h^{-1} (Figure 3b), while Ag/ZnO and Pd/ZnO produce CH_4 and CO without multi-carbon products (Figure 3c,d) [78].

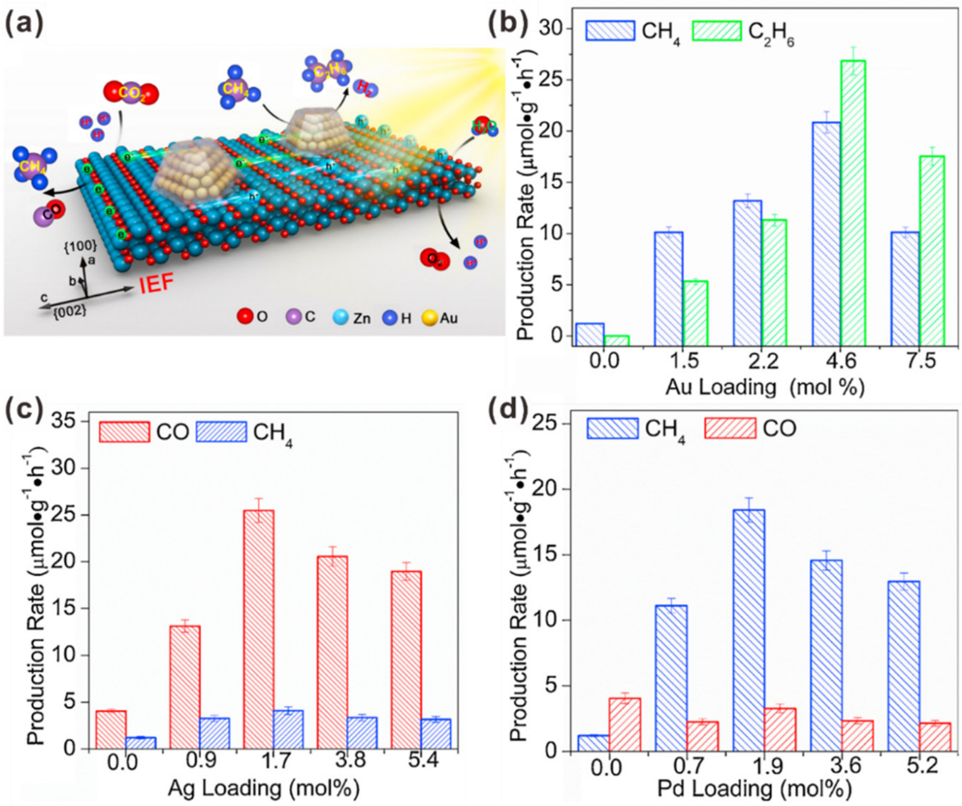

Figure 3. (**a**) Schematic illustration of the photocatalytic conversion of CO_2 to C_2H_6 using Au/ZnO nanosheets, and the hydrocarbon production rates from CO_2 with loading plasmonic metals of (**b**) Au, (**c**) Ag, and (**d**) Pd to ZnO. Reproduced with permission from Reference [78]. Copyright 2019 Elsevier.

Nguyen et al. used metal–organic frameworks (MOFs) with AuNPs for photocatalytic CO_2 conversion to methanol and ethanol [79]. They observed the effect of Au loading on the Au_x@zeolitic imidazolate framework (ZIF-67) for the reaction in which Au_{10}@ZIF-67 showed the highest performance of CH_3OH production at a rate of 1623 μmol g^{-1} h^{-1}, while Au_{20}@ZIF-67 showed that C_2H_5OH production occurred at a rate of 495 μmol g^{-1} h^{-1} (Figure 4a,b), and both CH_3OH and C_2H_5OH products decreased with Au_{30}@ZIF-67, possibly due to the agglomeration of AuNPs. Because the reaction to form C_2H_5OH requires more electrons than CH_3OH, these phenomena are thought to be the result of higher hot electrons that enable the photoreduction and support C_2H_5OH generation due to higher Au concentrations [79].

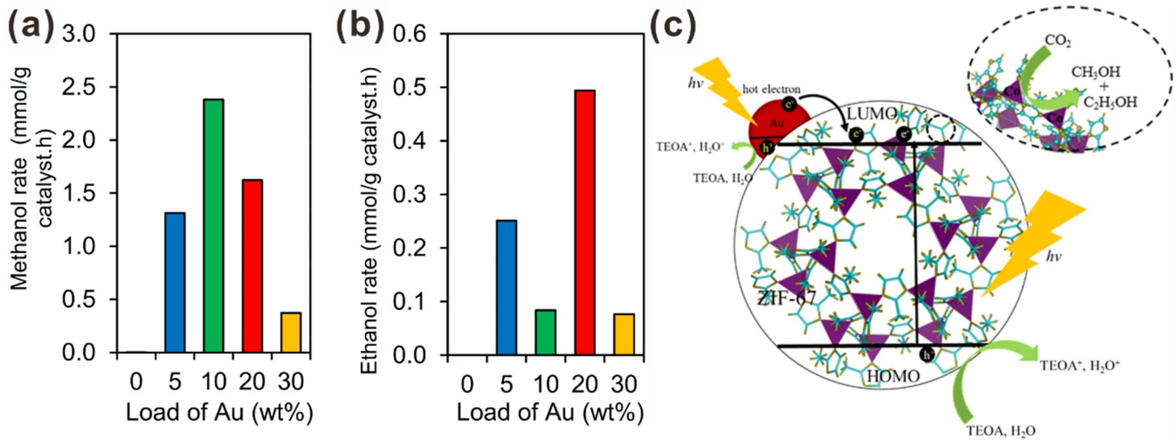

Figure 4. Photocatalytic activity of Au_x@ZIF-67 for CO_2 reduction to (**a**) CH_3OH and (**b**) C_2H_5OH, and (**c**) the mechanism of CO_2 photoreduction. Reproduced with permission from Reference [79]. Copyright 2020 American Chemical Society.

2.2. Silver Nanoparticle (AgNP)-Assisted Plasmonic Photocatalysts for CO_2 Reduction to Multi-Carbon Products

The silver nanoparticle (AgNP) is also one of the plasmonic materials that can exhibit unique optical properties for photocatalysts under visible light with LSPR, like AuNP [80]. Cai et al. prepared $AgCl_xBr_{1\text{-}x}$ alloy nanocrystals and found that the conduction band level could be affected by varying compositions [81]. The substitution of Cl with Br leads to a narrower band gap due to a negative shift in the conduction band minimum. Accordingly, $AgCl_{0.75}Br_{0.25}$ exhibited higher photocatalytic efficiency for CO_2 reduction into both CH_3OH (181 µmol g^{-1}) and C_2H_5OH (362 µmol g^{-1}) than any other $AgCl_xBr_{1\text{-}x}$ with different compositions. Furthermore, the amplified electric field due to the LSPR of Ag^0 species also contributes to the light enhancement by encouraging the photocatalytic reaction. Cai et al. further developed an Ag/AgCl photocatalyst system with a coaxial tri-cubic morphology, called red Ag/AgCl [82]. The enhancement of light harvesting property with red Ag/AgCl was observed, compared to normal AgCl, due to the synergistic effect between metallic AgNPs and the n-type AgCl semiconductor, which is the featured LSPR, Schottky junction, and polarization effect induced by surface plasmons. As a result, the CH_3OH and C_2H_5OH yields and apparent quantum efficiency for the red Ag/AgCl catalysts were 146 and 223 µmol g^{-1} for 5 h, respectively, in which both are higher than those for normal AgCl catalysts (Figure 5) [82].

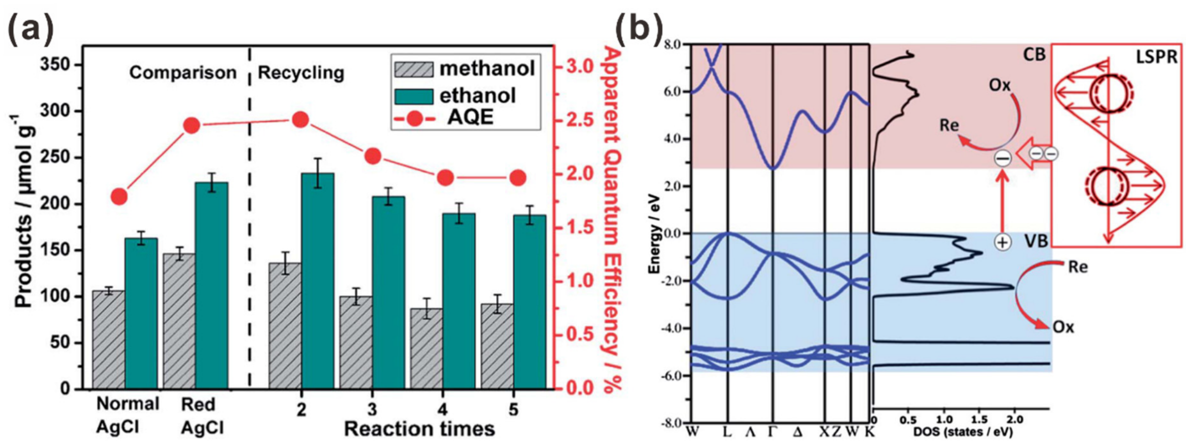

Figure 5. (**a**) The comparison of the photocatalytic efficiency for CO_2 reduction to CH_3OH and C_2H_5OH with red Ag/AgCl, and (**b**) a schematic illustration of physical photocatalytic mechanism. Reproduced with permission from Reference [82]. Copyright 2014 Royal Society of Chemistry.

Li et al. suggested a system with a plasmonic photocatalyst other than the C–C coupling of CO_2 alone by adopting the oxidative coupling of methane using CO_2 as the oxidant [83]. In the Ag/TiO_2 system, AgNPs can absorb visible light and generate hot electrons and holes, and the hot electrons are injected into TiO_2 while hot holes should be captured by CH_4. Otherwise, it will lead to the accumulation of Ag(I), which can be reduced back to Ag(0) under UV light. At the same time, TiO_2 can generate photoexcited electron–hole pairs, and photoexcited holes can combine with hot electrons from Ag, while photoexcited electrons can reduce CO_2 adsorbed on TiO_2. This synergistic effect enhances the photocatalytic activity of the reaction (1149 μmoL g^{-1} h^{-1} for CO and 686 μmol g^{-1} h^{-1} for C_2H_4) and contributes to the high stability of the catalyst (Figure 6b) [83]. They also demonstrated that other types of support materials with Ag did not present any synergistic effect due to the formation of an unsuitable Schottky barrier and CO_2 adsorption sites (Figure 6c), and other precious metals with TiO_2 showed lower activity for the photocatalytic reaction due to the poor SPR effect of the metals (Figure 6d) [83].

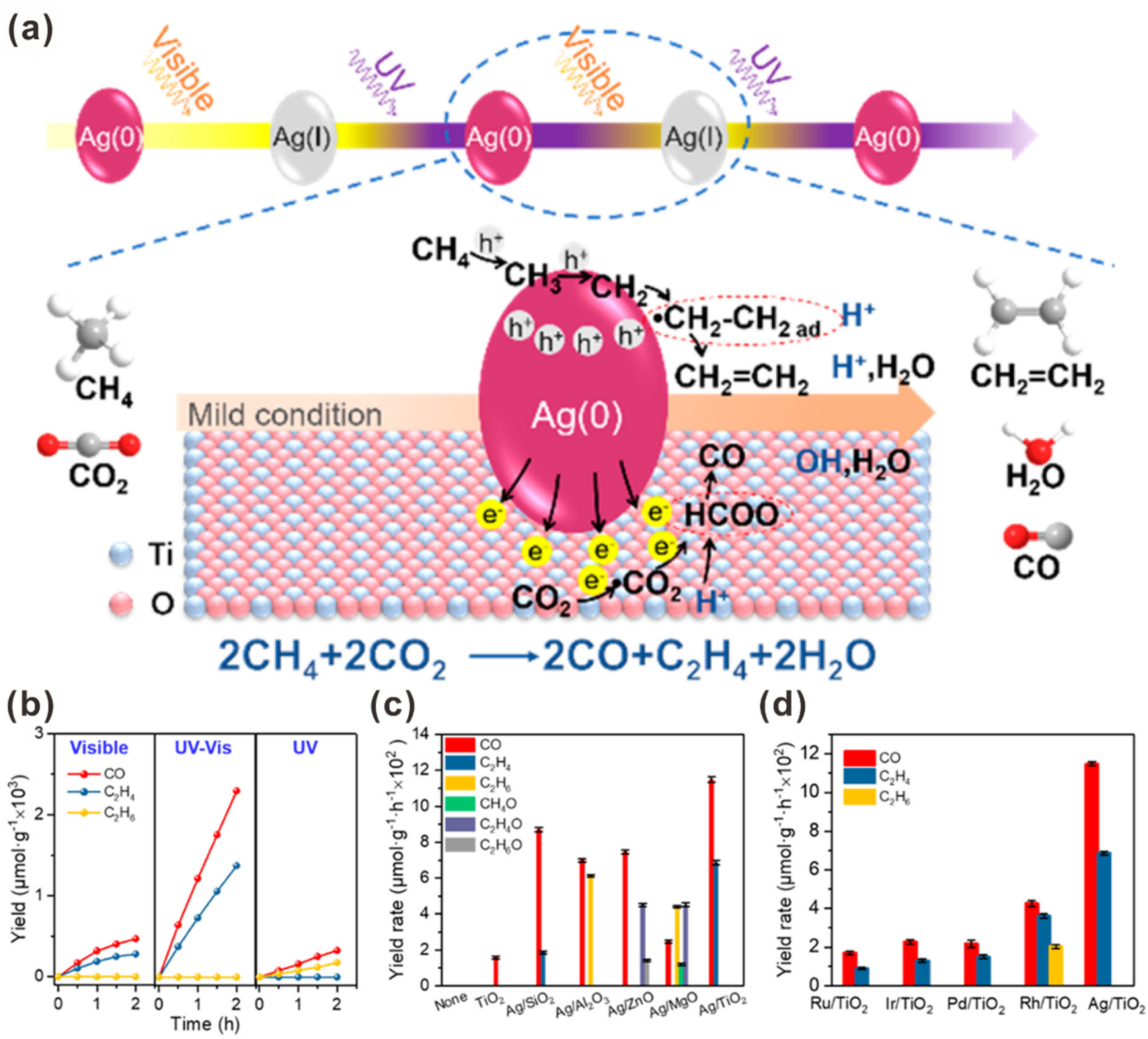

Figure 6. (**a**) Schematic illustration of Ag/TiO_2 for photocatalysis of CH_4 and CO_2 into ethylene and the photocatalytic performance depending on (**b**) the light source, (**c**) primary photocatalyst, and (**d**) metal cocatalyst. Reproduced with permission from Reference [83]. Copyright 2019 American Chemical Society.

2.3. Copper Nanoparticle (CuNP)-Assisted Photocatalytic CO_2 Reduction to Multi-Carbon Products

Metallic Cu species, including CuNPs, have been used as cocatalysts due to their known effectiveness in generating not only C_1 products, but also multi-carbon organic compounds, not as light absorbers with the LSPR effect [84–87]. Therefore, Cu has been used as an electron acceptor and suppressor of recombination of photoexcited electron–hole pairs generated from semiconductors [88–90]. Shown et al. prepared CuNP-decorated graphene oxide because of the large work function of Cu compared to that of GO, producing methanol and acetaldehyde [88]. They controlled the production rates and the ratio of and between both products by adjusting the work function of Cu/GO hybrids [88]. Park et al. used trititanate nanotubes (TNTs) decorated with Cu and CdS quantum dots (CdS/Cu-TNTs) for the production of C_1–C_3 hydrocarbons [89]. When irradiated with light, an efficient reduction of CO_2 to C_1–C_3 hydrocarbons was observed by the transport of photogenerated electrons to the Cu part through the TNTs while photogenerated holes oxidize water, which is similar to artificial photosynthesis [89]. Chen et al. carried out photocatalytic CO_2 reduction with benzyl alcohol oxidation to benzyl acetate using Cu_2O/Cu nanocomposites due to the narrow direct band gap and the position of the conduction band of Cu_2O [90]. Electrons and holes are generated over Cu_2O with visible light irradiation, and the electrons transfer to the surface of Cu due to their lower work function, while the holes can react with benzyl alcohol to form benzaldehyde, followed by the subsequent coupling reaction to form benzyl acetate [90]. CuNPs have great potential for photocatalytic C–C coupling, but more research is needed to utilize CuNPs for light harvesting materials.

There have been several attempts to produce value-added fuels through CO_2 conversion using plasmonic hybrid photocatalysts, even though only a few studies have been conducted to generate single carbon products. The hybrid structures of the photocatalysts, reaction conditions, and yields are summarized in Table 1.

Table 1. Plasmonic hybrid nano-catalysts for various photocatalytic CO_2 conversion into multi-carbon products. AuNP-, AgNP- and CuNP-assisted photocatalysts under visible light.

Photocatalyst	Size and Shape	Product	Light Source	Reaction Condition	Time	Yield (µmoL g^{-1} h^{-1})	Ref.
$Au@TiO_2$	Spherical core: 45 nm Spherical shell: 200–250 nm (50 nm thickness)	CH_4, C_2H_6	300 W Xe arc lamp	H_2O	10 h	2.52 (CH_4), 1.67 (C_2H_6)	[76]
AuNPs	11.8 ± 2.3 nm spherical NPs	CH_4, C_2H_6	300 W Xe lamp	10% IPA	10 h	0.65 (CH_4), 0.56 (C_2H_6) as TOF ($NP^{-1}h^{-1}$)	[77]
Au/ZnO	AuNPs: 7 nm ZnO sheets: >µm (1.6 nm thickness, 10–100 nm pores)	CH_4, C_2H_6	300 W Xe lamp (>320 nm)	H_2O	1–6 h	21.0 (CH_4), 27.0 (C_2H_6)	[78]
$Au_{20}@ZIF\text{-}67$	AuNPs: 30–40 nm ZIF-67: ~µm	CH_3OH C_2H_5OH	Solar simulator (150 mW cm^{-2})	10 wt.% TEOA, 0.08 M $NaHCO_3$	4 h	1623 (CH_3OH), 495 (C_2H_5OH)	[79]
$AgCl_{0.75}Br_{0.25}$	Cubic nanocrystals 150–260 nm	CH_3OH C_2H_5OH	500 W Xe arc lamp (>420 nm)	0.1 M $NaHCO_3$	5 h	36.2 (CH_3OH), 72.4 (C_2H_5OH)	[81]
Ag/AgCl	Coaxial tri-cubic 500–600 nm	CH_3OH C_2H_5OH	500 W Xe arc lamp (>420 nm)	0.1 M $NaHCO_3$	5 h	29.2 (CH_3OH), 44.6 (C_2H_5OH)	[82]
Ag/TiO_2	AgNPs: 4 nm TiO2: 25 nm	CO C_2H_4	Xe lamp	Quartz cotton, micro-autoclave	2 h	1149 (CO) 686 (C_2H_4)	[83]
Cu/GO	Cu (111) NPs: 5 nm GO: >µm	CH_3OH CH_3CHO	Halogen lamp (300 W)	Continuous gas flow reactor	2 h	2.94 (CH_3OH), 3.88 (CH_3CHO)	[88]
CdS/(Cu-TNTs)	Hexagonal CdS	CH_4 C_2H_6 C_3H_8	450 W Xe lamp (>420 nm)	H_2O	5 h	~28 (CH_4), ~17 (C_2H_6), ~9 (C_3H_8) µL g^{-1} h^{-1}	[89]
Cu_2O/Cu	Irregular porous structures 100 nm	Benzyl acetate	300 W Xe lamp (420–800 nm)	MeCN, benzyl alcohol	20 h	116.7	[90]

3. Plasmonic Hybrid Photocatalysts for C–C Cross-Coupling

The Suzuki–Miyaura coupling, which is one of the most powerful methods for carbon–carbon cross-coupling, is the reaction between an organoboron species and aryl halide in the presence of a palladium (Pd) catalyst and base [21,91]. Although most of this reaction involves a Pd catalyst, which has been regarded as a catalytically active site for the reaction, Pd is difficult to use as a photocatalyst because of its low absorption of visible light [92]. In recent years, to remedy this shortcoming, plasmonic nanoparticles and semiconductors that can absorb visible light have been used. In particular, plasmonic NPs (Au, Ag, Cu) are useful materials that can help the reaction of the Pd catalyst because they interact with visible light to show a strong LSPR phenomenon [93–95]. In addition, semiconductors are introduced into plasmonic materials, so-called plasmonic hybrid structures, to help plasmonic NPs extend the lifetime of hot electrons excited by light, or to form electron–hole pairs [96,97]. The hybrid structures classified by each type of plasmonic NPs for photocatalytic C–C cross-coupling reactions are described below.

3.1. AuNP-Assisted Plasmonic Photocatalysts for C–C Cross-Coupling

For C–C cross-coupling reactions, Au–Pd nanocomposites can be utilized, where the Au part absorbs visible light and transfers hot electrons into Pd, and the Pd part acts as electron acceptors and active sites. Some studies using Au–Pd alloys without non-plasmonic materials, such as AuPd nano-wheels [98] and AuPd nanotriangles [99] for photocatalytic C–C cross-coupling, have been reported (Figure 7). Huang et al. prepared AuPd nano-wheels, in which Pd encircles an Au core, with a controllable edge length and tunable SPR using a facile wet-chemical reduction method. In this work, the photocatalytic efficiency of the nano-wheel-catalysts for benzyl alcohol conversion and Suzuki coupling was confirmed, and the yield of products was 65.8% at 50 °C for 1 h under visible light (Figure 7a) [98]. Gangishetty et al. synthesized AuPd bimetallic nanotriangles consisting of an Au nanotriangle core with an unevenly distributed Pd shell, which is similar in morphology with AuPd nano-wheels [99]. The nano-catalysts showed >80% yield of Suzuki coupling between *p*-iodobenzoic acid and phenylboronic acid for 5 h under a green LED, accompanied by an increase in the temperature from 25 °C to 37 °C while the dark reaction showed only ca. 35% lower conversion compared to the light reaction (Figure 7b). Compared to the yield under dark reaction at 37 °C (ca. 75%), the pure photocatalytic effect is not significant, while the photothermal effect generated from non-radiative plasmon decay is the primary factor (Figure 7b) [99].

Sarina, Xiao et al. prepared Au–Pd alloy NPs embedded on ZrO_2, which has a band gap of approximately 5 eV, exhibiting negligible visible light absorption above 400 nm, so that the ZrO_2 support does not contribute to the photocatalytic activity of C–C cross-coupling (Figure 8) [100–103]. Several C–C coupling reactions such as Suzuki–Miyaura, Sonogashira, Stille, Hiyama, Buchwald–Hartwig, and Ullmann coupling, were conducted to study the effects of the wavelength and intensity of the light, the Au/Pd molar ratio of the alloy NPs on the photocatalytic activity, and the photocatalytic mechanism for the C–C coupling reactions. The researchers described the photocatalytic process in view of reaction kinetics. The reduced activation energy for the C–C coupling reaction is possible by visible-light absorption of photocatalyst, indicating the low activation energy in the photocatalytic process compared with that of a thermal reaction process (Figure 8b,c) [101,102]. In terms of energy levels of the molecular orbital, there are two light absorption mechanisms such as inter-band excitation and LSPR absorption at 530 nm for AuNPs. Inter-band excitation is possible with short-wavelength (e.g., 400 nm) absorption via a single-electron excitation. When irradiated with short-wavelength, single-photon excitation generates hot electrons to be injected into the lowest unoccupied molecular orbital (LUMO). In the case irradiated with longer wavelengths, the hot electrons generated by the collective excitation of LSPR can only induce reactions with lower energy thresholds (Figure 8d) [103]. In spite of the low TOF and the number of conversion reactions, they provided a comprehensive insight for the photocatalytic reactions for various C–C cross-coupling reactions and explained the kinetics and mechanisms of the reactions.

Other researchers have used a variety of support materials such as semiconductors (e.g., CeO_2, graphitic carbon nitride (g-C_3N_4)) [104,105], metal–organic frameworks (MOF, UiO-66-NH_2) [106], polymers (e.g., perylene bisimide (PBI), polystyrene) [107,108], wide band gap semiconductors (TiO_2) [109–112], and silica [113]. Semiconductors that have narrower band gaps than 3.1 eV (i.e., 2.7 eV for g-C_3N_4) can absorb visible light to generate electron–hole pairs, which are transferred to metal NPs. By itself, a semiconductor can help the Pd catalyst in photocatalytic C–C cross-coupling reactions [114–116], but even the synergy of plasmonic hybrid with semiconductors can be expected to have greater photocatalytic efficiency for a C–C cross-coupling reaction. In these systems, the hot electrons generated from AuNPs (due to the strong LSPR effect of AuNPs) using irradiation can be injected into the attached Pd, in which the electrons transfer to aryl halide molecules, while the photogenerated electron–hole pairs of semiconductors by irradiation can be separated, causing electrons to recover into the Au^0 state and holes to transfer into solvent or phenylboronic acid to be activated (Figure 9) [104,105]. Moreover, semiconductors such as g-C_3N_4 are two-dimensional materials with large surface areas and unique electronic/optical properties, and Schottky junctions form at the interface of the metal and semiconductor, relying on the band alignment and work function [114–116], leading to a positive effect on catalytic efficiency (Figure 9b) [105]. Therefore, the AuPd/g-C_3N_4 nanohybrid showed a very high TOF of 7920 h^{-1} in the C-C cross-coupling reaction.

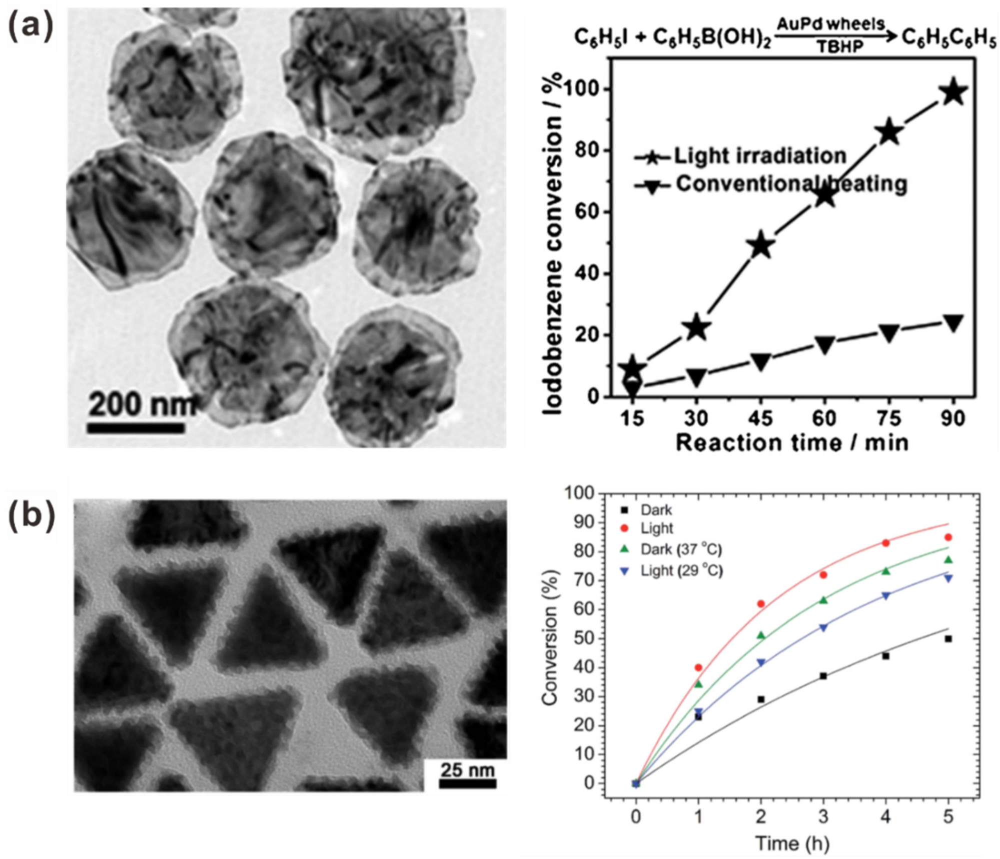

Figure 7. Au–Pd bimetallic alloys for photocatalytic Suzuki coupling. (**a**) AuPd nano-wheels. Reproduced with permission from Reference [98]. Copyright 2013 Wiley-VCH. (**b**) AuPd nanotriangles. Reproduced with permission from Reference [99]. Copyright 2017 Royal Society of Chemistry.

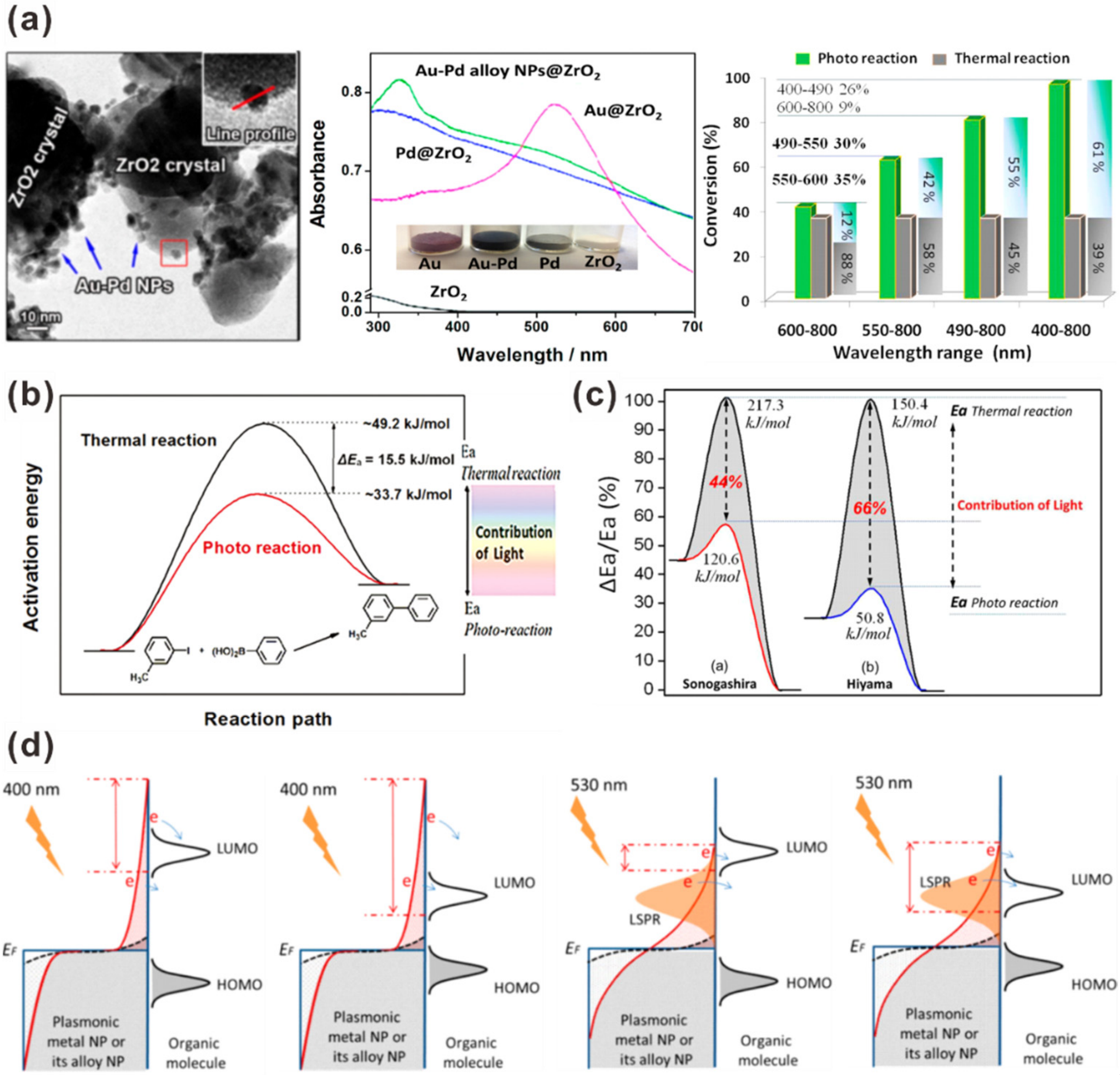

Figure 8. Au-Pd alloy nanoparticles (NPs) embedded on ZrO_2 for visible-light-induced photocatalytic C–C cross-couplings. (**a**) Morphology, characterization, and photocatalytic efficiency of Suzuki coupling. Reproduced with permission from Reference [100]. Copyright 2013 American Chemical Society. Apparent activation energies of (**b**) Suzuki, (**c**) Sonogashira, and Hiyama couplings calculated for the photoreaction and the reaction in the dark. Reproduced with permission from References [101,102]. Copyright 2014 Royal Society of Chemistry. Copyright 2014 American Chemical Society. (**d**) The distribution of hot electron in the plasmonic metal or its alloy NPs with 400 nm, 530 nm irradiation, and their contribution to quantum efficiency. Reproduced with permission from Reference [103]. Copyright 2017 American Chemical Society.

MOFs such as UiO-66-NH_2 are similar to semiconductors in that they have a band gap (approximately 2.67 eV) capable of absorbing visible light. The key differences are that the energy transfer occurs from ligands to a metal. The pore volume and surface area can be controlled by using the functional group. Noble metals can be introduced into MOFs, and they exhibit high dispersion stability owing to the ultra-high surface area [106].

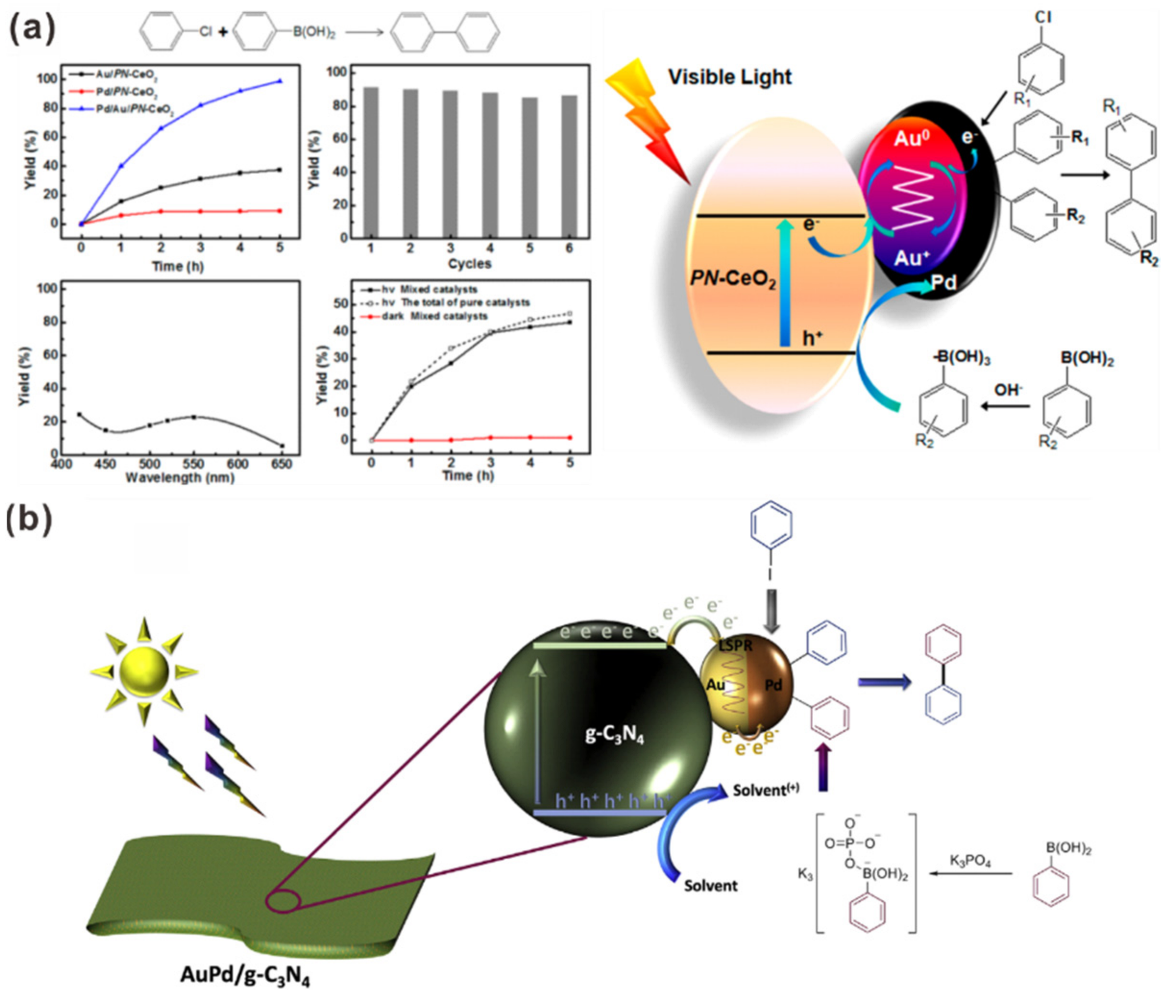

Figure 9. AuPd NPs decorated semiconductors for photocatalytic Suzuki coupling under visible light. (**a**) Pd/Au/CeO_2. Reproduced with permission from Reference [104]. Copyright 2015 American Chemical Society. (**b**) AuPd/g-C_3N_4. Reproduced with permission from Reference [105]. Copyright 2020 Elsevier.

In general, wide band gap semiconductors such as TiO_2 display great light absorption at wavelengths below 400 nm, making it difficult to expect visible light absorption for catalytic reactions [37]. Furthermore, the high energy of UV light might oxidize and reduce organic reactants, which can result in low yield and selectivity. Rohani et al. changed the morphology of TiO_2 into urchin-like yolk–shell structures with unique properties, such as a high surface area and visible-light harvesting (Figure 10) [112]. The hydrogenated urchin-like yolk@shell TiO_2 structure (HUY@S-TOH) was decorated with plasmonic Au/Pd NPs for photocatalytic Suzuki coupling. The structure showed absorption property for visible light because of the Ti^{3+} species on the surface of the structure and AuNPs, enhancing the light harvesting efficiency and the inhibition of the recombination of photogenerated electron–hole pairs by decreasing the band gap of TiO_2 to the visible region. In addition to the strong interaction between noble metals and TiO_{2-x}, HUY@S-TOH/AuPd showed a high catalytic efficiency with a TOF value of 7095 h^{-1}.

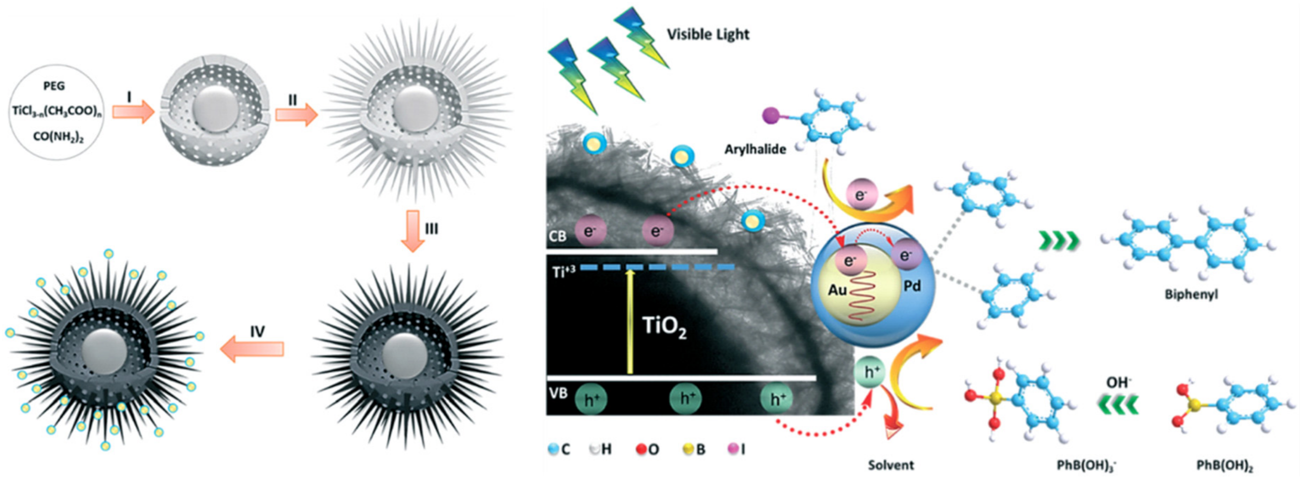

Figure 10. The HUY@S-TOH/AuPd for visible-light-driven photocatalytic Suzuki coupling. Reproduced with permission from Reference [112]. Copyright 2019 Royal Society of Chemistry.

Graphene and its derivatives are 2D materials with an exceptional electron mobility of 2×10^5 $cm^2{\cdot}v^{-1}s^{-1}$ and variable band gap that depends on the oxidation state of graphene [69,117,118]. Hybrid structures containing graphene or its oxide have been reported for photocatalytic C–C cross-coupling to extend the lifetime of hot electrons of plasmonic NPs generated by light absorption or to prevent recombination of electron–hole pairs [119,120]. Moreover, graphene or slightly oxidized graphene on its own can also be a good support material not only for combination with Pd^{2+} or Pd^0 NPs owing to its functional group, but also for transferring electrons into Pd with facilities to enhance catalytic activity [121]. Kang et al. studied the effect of interfaces on Pd-nanodot-decorated AuNPs with a graphene layer with different oxidation states for photocatalytic Suzuki coupling (Figure 11) [119]. They prepared Pd-cys-AuNPs, Pd-GO-AuNPs, and Pd-rGO-AuNPs with different oxidation states, and found that Pd-rGO-AuNPs exhibited the fastest reaction progress (66.4% with a thermal effect and 54.4% without a thermal effect), while the Pd-cys-AuNPs exhibited the slowest reaction progress (30% with a thermal effect and 6.7% without a thermal effect) for 2 h (Figure 11b,c). The contribution of the electron transfer mechanism from plasmonic NPs (AuNPs) to Pd nanodots is significant through the graphene interface, preventing the relaxation of hot electrons of plasmonic NPs induced by light [119].

Plasmonic properties can be tuned by size and shape by utilizing varying wavelengths of light [46,122]. Gold nanorods (AuNRs), like spherical AuNPs and other noble metal NPs, have the ability to interact with light of varying wavelengths through LSPR [46,123–125]. They display two SPR bands of transverse and longitudinal bands due to their anisotropic shape. The transverse mode is located near 500 nm, while the longitudinal mode varies widely depending on the aspect ratio and the overall size of AuNRs, generally located in the NIR region. Therefore, AuNRs have been used as NIR-responsive photocatalysts [122,126].

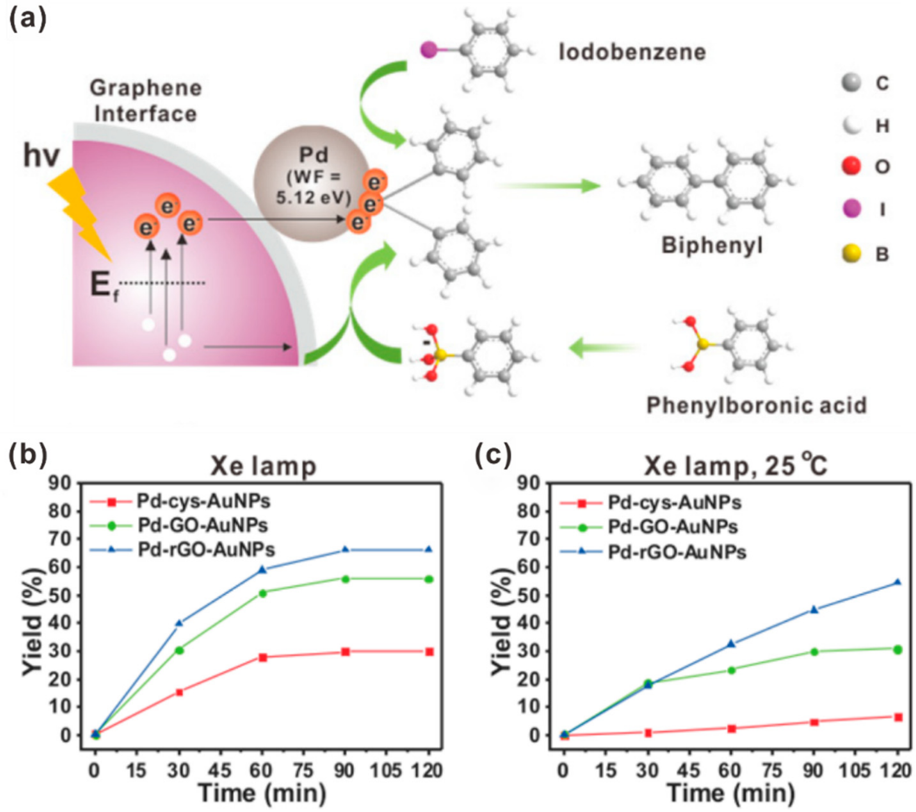

Figure 11. Pd-nanodot-decorated AuNPs with a graphene interface for visible-light-induced photocatalytic Suzuki–Miyaura coupling reaction. (**a**) The scheme of the Suzuki–Miyaura cross-coupling with Pd nanodot-decorated AuNPs and (**b**,**c**) the catalytic activities of Pd-cys-AuNPs, Pd-GO-AuNPs, and Pd-rGO-AuNPs for the reaction under various conditions. Reproduced with permission from Reference [119]. Copyright 2018 Creative Commons Attribution.

AuNR-based photocatalysts have been applied to C–C coupling reactions [127–131]. Wang et al. synthesized Au–Pd nanostructures where Pd NPs were located at the tip of the AuNRs to a large extent as well as on the whole surface of the AuNRs (Figure 12a). They conducted photocatalytic Suzuki coupling under an 809-nm laser in the NIR region, yielding biphenyl products, where they demonstrated the two origins of the catalytic activity of Au–Pd nanostructures, which is the plasmonic heating process and plasmon-excitation-induced hot electrons [127]. Guo et al. developed Au–Pd nanostructures, called Au@Pd superstructures formed from different directing agents, investigating the effect of the shapes of Pd, which are superstructures, nano-dendrites, and shell structures (Figure 12b). Different from AuNRs, the Au@Pd core@shell exhibited weak electric field enhancement due to the plasmon shielding effect of Pd shells. In the case of Au@Pd nano-dendrites with discrete Pd surfaces, the $|E|/|E_0|$ around their surface was largely enhanced by 16 of the maximum value of $|E_{max}|/|E_0|$, which allows the inside of the AuNR core to be excited partially. The Au@Pd superstructures displayed further improvement of $|E_{max}|/|E_0|$ up to 23 because of the ordered open structure of the Pd nano-arrays and their strong plasmonic antenna effect. Accordingly, the plasmon-enhanced photocatalytic activity of Au@Pd superstructures was >4 times higher than that of the Au@Pd core@shell (TOF $\approx$ 2880 h^{-1}), and approximately two times higher than that of the Au@Pd nanodendrites [129]. Yoshii et al. designed Pd-graphene-AuNR nanocomposite catalysts similar to Pd-rGO-Au by Kang et al., facilitating the transfer of SPR-induced hot electrons by AuNR to the catalytic active metals (Pd) through the graphene layer (Figure 12c). Almost all aspects of Pd-graphene-AuNR nanocomposites are similar to Pd-rGO-Au, and the only difference is that AuNR was used to absorb NIR light [131].

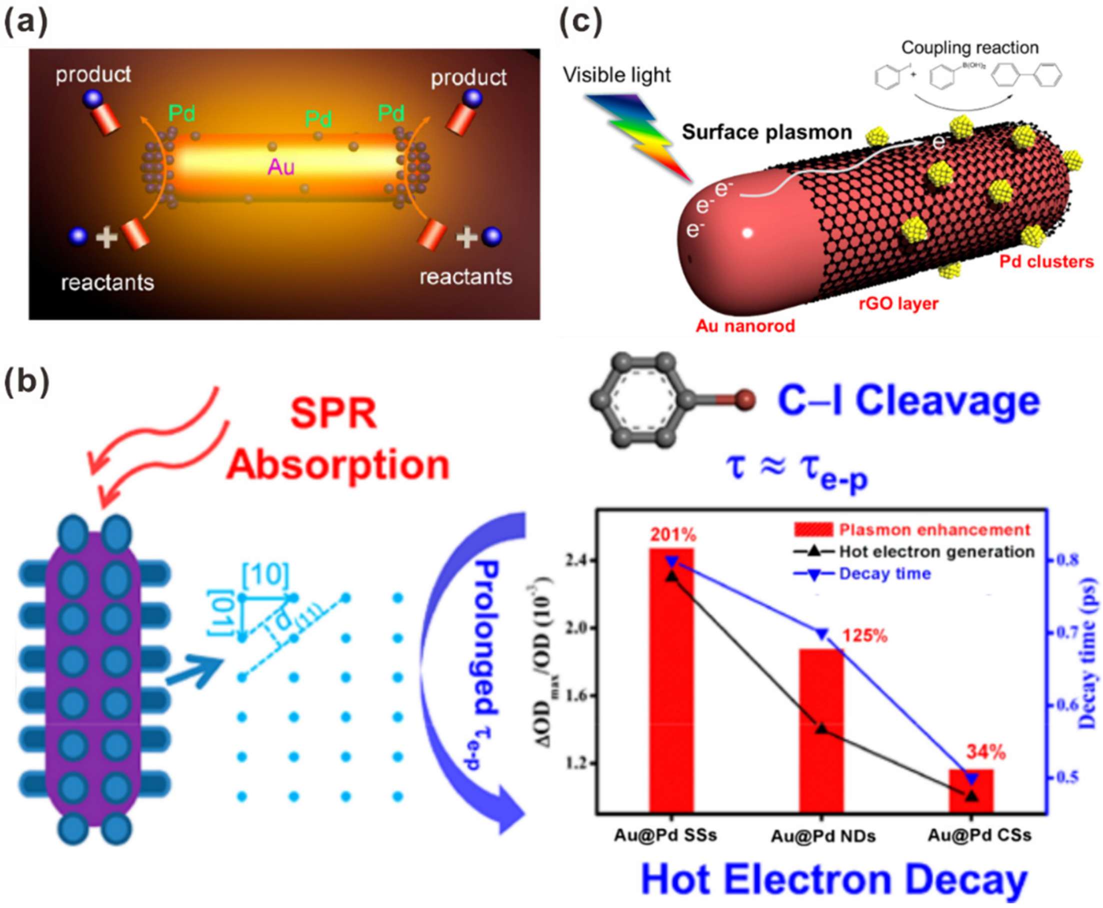

Figure 12. NIR-light-induced plasmonic photocatalysts for C–C cross-coupling. (**a**) Au–Pd nanostructures. Reproduced with permission from Reference [127]. Copyright 2013 American Chemical Society. (**b**) AuNR@Pd superstructures. Reproduced with permission from Reference [129]. Copyright 2017 American Chemical Society. (**c**) Pd-graphene-AuNR nanocomposites. Reproduced with permission from Reference [131]. Copyright 2019 American Chemical Society.

3.2. AgNP-Assisted Plasmonic Photocatalysts for C–C Cross-Coupling

AgNP-based hybrid photocatalysts with various support materials such as graphene oxide with AgBr [132], silica [113,133], supramolecular ensemble with Cu_2O [134,135], and TiO_2 [136] for C–C cross-coupling have been reported. Verma et al. used mesoporous silica as a support material (SBA-15, Aldrich), of which the channel can contain Pd/Ag NPs with stability for photocatalytic Suzuki coupling [113,133]. They observed the effect of the shape of Ag or type of plasmonic NPs (Au or Ag), affecting plasmonic optical properties and catalytic activity (Figure 13). They found that longer aspect ratios of the Ag nanostructure result in higher photocatalytic activity efficiency due to the light absorption property (<30% for Pd/Ag/SBA-15(Y), ~40% for Pd/Ag/SBA-15(R), 53% for Pd/AgSBA-15(B)) (Figure 13b) [133]. Although the photocatalytic activity for Suzuki coupling with Pd/Au/SBA-15 was better than that for Suzuki coupling with Pd/Ag/SBA-15 (~70% for Pd/Au/SBA-15, and ~40% for Pd/Ag/SBA-15) (Figure 13d), the activity with Pd/Ag/SBA-15 for the dehydrogenation reaction was better than that with Pd/Au/SBA-15, indicating that it is difficult to simply compare the effects of those reactions [113]. Putting it all together, it is meaningful that Ag and Au can work complementarily with each other in terms of light absorption.

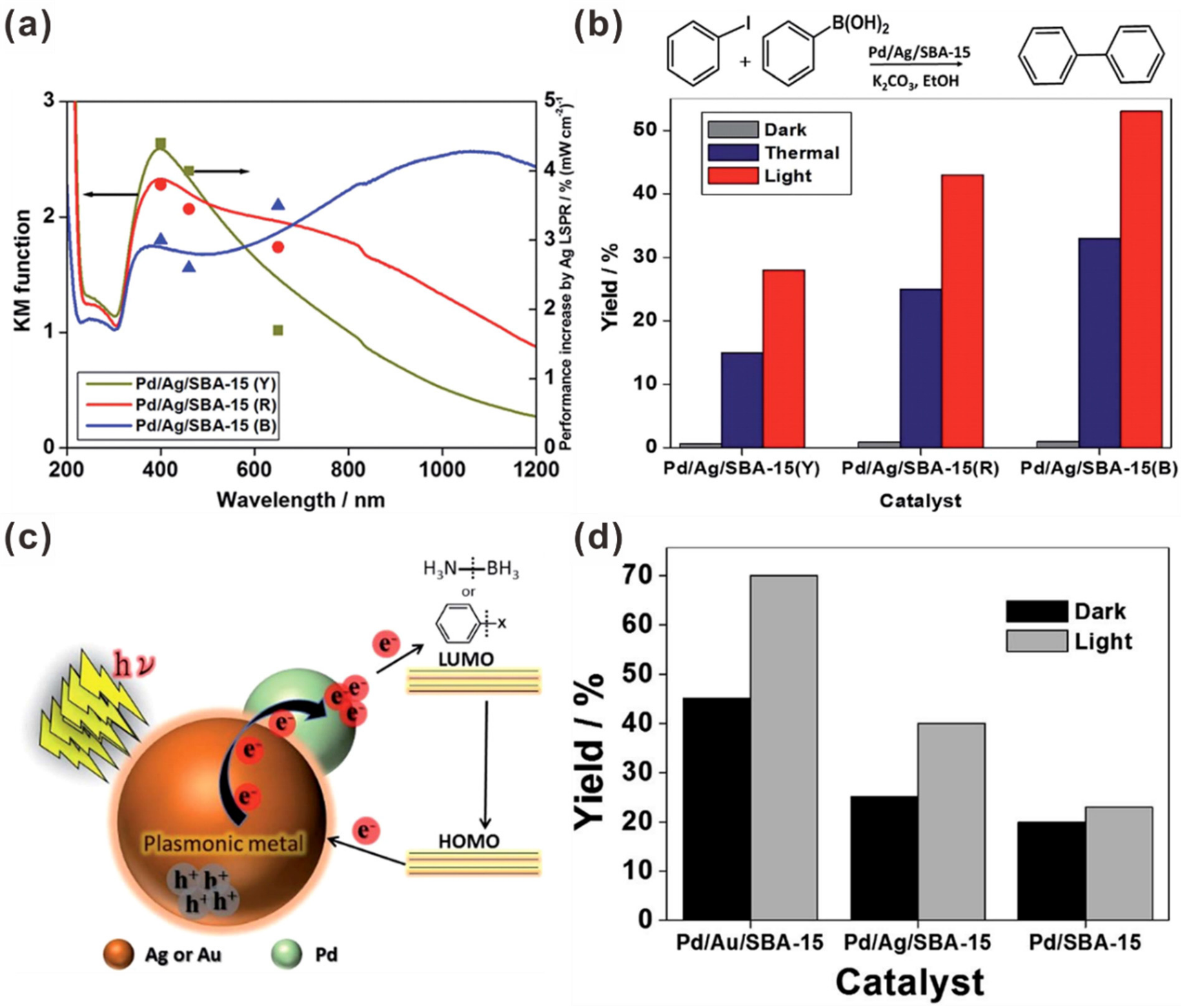

Figure 13. Pd/Ag bimetallic nano-catalysts on mesoporous silica for photocatalytic Suzuki coupling. (**a**) UV-vis spectra and wavelength dependence of the photocatalysts, (**b**) the catalytic activities of Pd/Ag/SBA-15 catalysts with different SBA-15, (**c**) the mechanism for the enhanced photocatalytic activity, and (**d**) the catalytic activities of Pd/metal/SBA-15. Reproduced with permission from References [113,133]. Copyright 2015 and 2016 Royal Society of Chemistry.

Bhalla's group used supramolecular ensembles as both reactors and stabilizers of NPs to a higher extent through electron-rich assemblies and introduced Cu_2O as a shell around the AgNP for its affordable price, stability, and property. Cu_2O is a p-type semiconductor and has been used as an efficient catalyst for C–C, C–N, and C–O cross-coupling reactions (Figure 14) [134,135]. These reports are not studies for the development of conventional Suzuki coupling, but they are significant in that they were performed without palladium even though they showed relatively low photocatalytic efficiency.

3.3. CuNP-Assisted Plasmonic Photocatalysts for C–C Cross-Coupling

Copper nanoparticles (CuNPs) are plasmonic materials like AuNPs and AgNPs, which possess unique optical properties [137–139]. However, their instability and tendency to undergo surface oxidation make it difficult for many researchers to utilize CuNPs [140]. Nevertheless, there have been some attempts to overcome the instability in order to use CuNPs for photocatalysts because of their low cost [141–143].

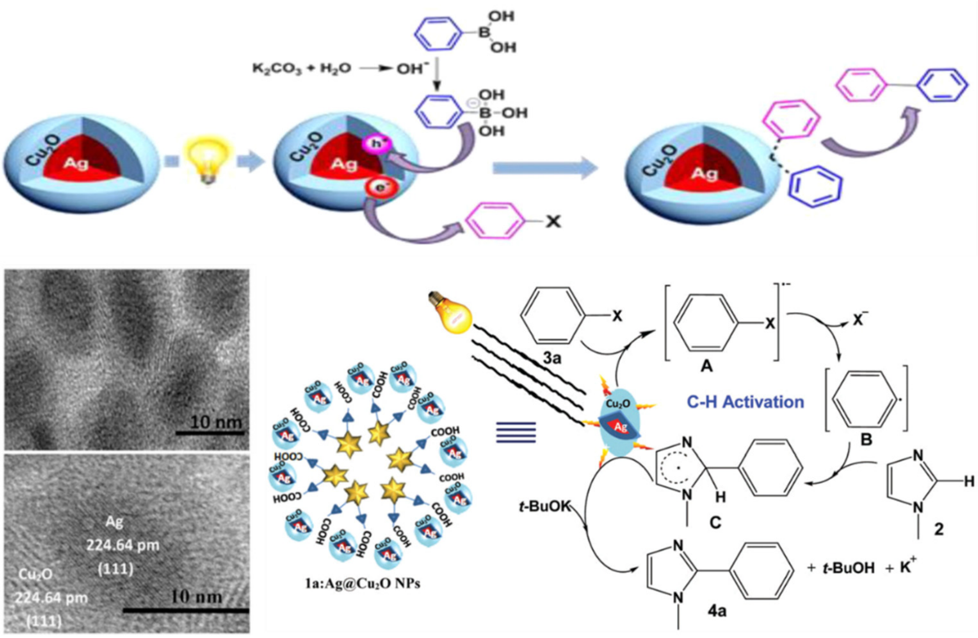

Figure 14. Ag@Cu$_2$O core–shell nanoparticles (NPs) stabilized by a supramolecular ensemble for photocatalytic Suzuki coupling. Reproduced with permission from References [134,135]. Copyright 2015 and 2016 Royal Society of Chemistry.

For C–C cross-coupling with CuNPs, CuPd bimetallic alloy NPs with other light-absorbing materials such as silicon carbide (SiC) as a semiconductor and NH_2-UiO-66(Zr) as MOF were used under visible light (Figure 15) [144,145]. Wang et al. prepared PdCu/SiC using a sol-gel and carbon thermal reduction process for photocatalytic Sonogashira reaction under visible light. They proposed a mechanism in which photogenerated electrons transfer to the Pd part, facilitating the cleavage of aryl halides, while photogenerated holes in the CuNPs react with phenylacetylene to form a phenylethynylcopper(I) compound (Figure 15a) [144]. Sun et al. prepared CuPd@NH_2-UiO-66(Zr), with encapsulated bimetallic CuPd nanoclusters inside the cavities of NH_2-UiO-66(Zr) via double-solvent impregnation followed by chemical reduction for a Suzuki coupling reaction. The transfer of the photogenerated electrons from the photoexcited NH_2-UiO-66(Zr) to the Pd part to form electron-rich Pd was facilitated by metallic Cu acts as an electron mediator, which results in the superior activity of photocatalytic Suzuki coupling, since Cu has a higher Fermi energy level as compared to Pd and lower Fermi energy level as compared to NH_2-UiO-66(Zr) (Figure 15b) [145]. These reports do not state the plasmonic light-harvesting property of CuNP itself as a photocatalyst, but attempts to introduce copper into Pd.

In order to stabilize CuNPs, Cui et al. introduced graphene to Cu because of the possible change of the electronic structure of Cu by the carbon vacancies or dangling bond in graphene [146,147]. Due to the LSPR effect of CuNPs, the electron density in Cu is polarized, causing charge heterogeneity at the surface of CuNPs with both relatively electron-rich sites and positively charged sites. The electron-rich sites can easily adsorb imidazole molecules and inject into the molecules, facilitating the cleavage of N–H bonds, while positively charged sites can assist to cleave C–B bonds in phenylboronic acid molecules, and, as a result, C–N bonds are formed (Figure 16a). Furthermore, graphene can also absorb light, generating a strong photocurrent, and the work function of graphene, which is lower than that of Cu, causes hot electrons to transfer to Cu from graphene easily, which can result in the collection of energetic electrons at the Cu sites to accelerate the reaction [147]. Bhalla et al. used supramolecular ensembles as reactors and stabilizers of CuNPs, which is similar to supramolecular ensemble-based Ag@Cu_2O core@shell NPs [148]. They confirmed the existence of the LSPR band of CuNPs for plasmonic photocatalysts, and the hybrid systems showed efficient photocatalytic efficiency for photocatalytic C(sp^2)–H alkynylation (another type of C–C coupling reaction) (Figure 16b). These reports are not about the named C–C cross-coupling reactions, but they are meaningful in that they make good use of the plasmonic properties of CuNPs as a photocatalyst.

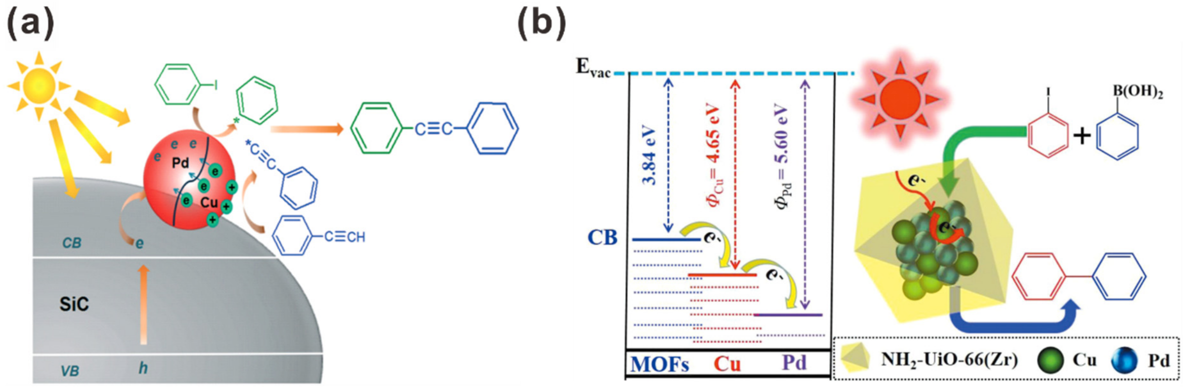

Figure 15. The schematic diagram of the proposed mechanism using CuPd bimetallic alloy for photocatalytic C–C cross-coupling. (**a**) PdCu/SiC for photocatalytic Sonogashira reaction. Reproduced with permission from Reference [144]. Copyright 2018 Royal Society of Chemistry. (**b**) CuPd@NH_2-UiO-66(Zr) for photocatalytic Suzuki coupling. Reproduced with permission from Reference [145]. Copyright 2018 Wiley-VCH.

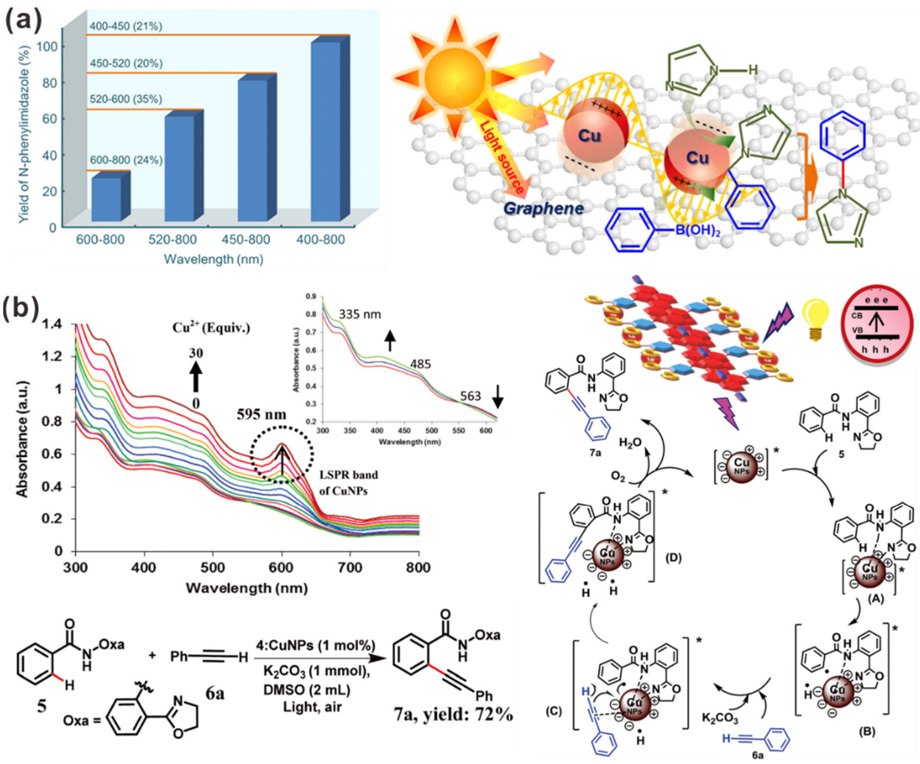

Figure 16. Plasmonic CuNPs with other support materials for photocatalysis. (**a**) Cu/graphene for photocatalytic C-N cross-coupling reaction. Reproduced with permission from Reference [147]. Copyright 2015 Nature Publishing Group. (**b**) Supramolecular ensemble 3:CuNPs for photocatalytic C-C cross-coupling by C(sp^2)-H functionalization. Reproduced with permission from Reference [148]. Copyright 2016 Royal Society of Chemistry.

Many attempts have been made to introduce Pd NPs into solid supports to stabilize or assist Pd for catalytic efficiency of C–C cross-coupling, in addition to the examples mentioned above. The hybrid structures of the plasmonic photocatalysts used, reaction conditions, and yields with TOF values for C–C cross-coupling are classified and summarized in Table 2.

Table 2. Plasmonic hybrid nano-catalysts for various photocatalytic C–C cross-coupling. AuNP-, AgNP-, CuNP-assisted photocatalysts under visible and NIR light.

Photocatalyst	Size and Shape	Reaction	Light Source	Reaction Temp.	Solvent, Base	Time	Yield	TOF (h^{-1})	Ref.
AuPd wheels	Nano-wheels 290 nm (6 nm thickness)	Suzuki	Xe lamp	50 °C	$EtOH/H_2O$ (9:1), K_2CO_3	1 h	65.8%	-	[98]
AuPd nanotriangles	Nanotriangles 43 ± 4 nm	Suzuki	Green LED (450–600 nm)	-	$EtOH/H_2O$ (1:6), K_2CO_3	5 h	>80%	-	[99]
Au–Pd alloy NPs/ZrO_2	Au-Pd NPs: <8 nm	Suzuki	500 W halogen lamp (400–750 nm)	30 °C	DMF/H_2O (3:1), K_2CO_3	6 h	96%	14.5	[100]
Au–Pd alloy NPs/ZrO_2	Au-Pd NPs: <7 nm	Sonogashira or Stille	Halogen lamp (400–750 nm)	45 °C	H_2O, K_3PO_4 or NaOH	24 h	80% −81%	4.7 −4.8	[102]
Au–Pd alloy NPs/ZrO_2	Au-Pd NPs: <7 nm	Suzuki	Halogen lamp (400–750 nm)	30 °C	DMF/H_2O (3:1), K_2CO_3	6 h	96%	14.5	[101]
Pd/Au/CeO_2	AuNPs (111): 4.28 ± 1.05 nm PdNPs (111): 5.14 ± 1.01 nm CeO_2 nanorods: ~5 nm (width), ~30 nm (length)	Suzuki	150 W Xe lamp (>400 nm)	25 °C	DMF/H_2O (1:1), K_2CO_3	5 h	98.8%	-	[104]
Pd/Au/SBA-15	Pd/Au NPs: 4.9 nm SBA-15: >µm	Suzuki	Xe lamp	Room Temp.	EtOH K_2CO_3	2 h	70%	-	[113]
Au–Pd alloy NPs/TiO_2	Au-Pd NPs: 3 nm	Suzuki	5 W blue LED lamp	25 °C	$EtOH/H_2O$ (1:1), K_2CO_3	5 h	98%	-	[109]
Pd-rGO-AuNPs	Pd nanodots: 2–3 nm AuNPs: ~30 nm	Suzuki	Xe lamp (400–800 nm)	25 °C	$EtOH/H_2O$ (1:1), K_2CO_3	2 h	54.5%	-	[119]
Au–Pd/HPS	AuNPs core: ~4 nm Pd shell: <1 nm HPS: 15–50 nm	Suzuki	300 W filament lamp	60 °C	$EtOH/H_2O$ (5:1), NaOH	3 h	71.6%	130.7	[108]

Table 2. *Cont.*

Photocatalyst	Size and Shape	Reaction	Light Source	Reaction Temp.	Solvent, Base	Time	Yield	TOF (h^{-1})	Ref.
TiO_2 + $PdAu/Al_2O_3$	-	Ullmann	Xe lamp (≥350 nm)	Room Temp.	CH_3CN	0.5 h	2.2%	-	[110]
TiO_2 + $PdAu/Al_2O_3$	PdAu NPs: 3–4 nm	Dehydrogenative cross-coupling	Xe lamp (≥350 nm)	Room Temp.	-	1 h	15.2 µmol	-	[111]
Supramolecular Polymer 5:AuNPs	Supramolecule: ~µm AuNPs: <30 nm	Heck	100 W tungsten filament blub	Room Temp.	H_2O, K_2CO_3	1 h	89%	-	[107]
GO/LDH @AuPd	AuPd NPs: ~4.2 nm	Suzuki	300 W Xe lamp (≥420 nm)	25 °C	$EtOH/H_2O$ (3:1), K_2CO_3	2 h	99.5%	-	[120]
HUY@S-TOH/AuPd	AuNPs core: 5 nm Pd shell: ~0.7 nm HUY@S-TOH: ~3 µm	Suzuki	300 W Xe lamp	Room Temp.	$EtOH/H_2O$ (2:1), K_2CO_3	0.5 h	>99%	7095	[112]
Au/Pd@UiO-66-NH_2	Au/Pd NPs: 6.45 nm UiO-66-NH_2: ~50 nm	Suzuki	300 W Xe lamp (>420 nm)	25 °C	$EtOH/H_2O$ (1:1), K_2CO_3	1 h	>99%	433	[106]
AuPd/g-C_3N_4	AuPd NPs: 5 nm	Suzuki	5 W Xe HID lamp	25 °C	$EtOH/H_2O$ (1:1), K_3PO_4	0.5 h	99%	7920	[105]
Au–Pd nanostructures	AuNRs: 25 ± 2 (diameter), 82 ± 6 nm (length) PdNPs: 3–5 nm	Suzuki	Continuous semiconductor laser (809 nm)	Room Temp.	H_2O, NaOH	1 h	99%	162	[127]
Pd-Au/SiO_2	AuNRs: ~10 nm (diameter), ~40 nm (length)	Suzuki	500 W Xe lamp (>420 nm)	Room Temp.	EtOH	0.5 h	78%	334	[128]
Au nanorod@Pd superstructures	AuNRs: ~20 nm (diameter), ~60 nm (length) Pd: 3.8 ± 0.1 nm	Suzuki	300 W Xe lamp (>510 nm)	40 °C	$EtOH/H_2O$ (1:3), NaOH	0.5 h	-	~2880	[129]
Au@Pd NRs	AuNRs: 49 ± 5 nm (diameter), 107 ± 8 nm PdNPs: ~5 nm	Suzuki	Continuous 808-nm laser	-.	H_2O, NaOH	1 h	97.6%	-	[130]

Table 2. *Cont.*

Photocatalyst	Size and Shape	Reaction	Light Source	Reaction Temp.	Solvent, Base	Time	Yield	TOF (h^{-1})	Ref.
Pd/Au@rGO-10/SiO_2	AuNRs: 25 nm (diameter), 75 nm (length) rGO layer: 2.8 nm Pd: 1.4 nm	Suzuki	500 W Xe lamp (>420 nm)	-	EtOH, K_2CO_3	0.5 h	56%	-	[131]
GO-Pd@Ag-AgBr	>µm	Suzuki	300 W Xe lamp (>400 nm)	25 °C	EtOH/H_2O (1:1), K_2CO_3	0.5 h	97%	-	[132]
Pd/Ag/SBA-15	Spherical AgNPs: ~4 nm Ag nanorods: ~10 nm	Suzuki	500 W Xe lamp (>420 nm)	35 °C	EtOH, K_2CO_3	6 h	53%	489	[133]
Pd/Ag/SBA-15	Pd/Ag NPs: 4.2 nm SBA-15: >µm	Suzuki	Xe lamp	Room Temp.	EtOH K_2CO_3	2 h	40%	-	[113]
Supramolecular ensemble-based Ag@Cu_2O NPs	AgNPs core: 10–15 nm Cu_2O shell: 10–15 nm thickness	Suzuki	100 W tungsten filament bulb	Room Temp.	EtOH/H_2O (3:1), K_2CO_3	5 h	75%	-	[134]
Supramolecular ensemble-based Ag@Cu_2O NPs	AgNPs core: 7.5 nm Cu_2O shell: 2.5 nm thickness	C-H activation	100 W tungsten filament bulb	Room Temp.	Toluene/H_2O (3:7), KO^tBu	5.5 h	80%	-	[135]
Ag/TiO_2	AgNPs: 1.5–5 nm TiO_2: 10-15 nm pores	Suzuki	20 W white LED (>420 nm)	Room Temp.	Toluene	24 h	97%	-	[136]
Cu/graphene	CuNPs: ~15 nm	C-N cross-coupling	300 W Xe lamp (400–800 nm)	Room Temp.	MeOH	1 h	99%	25.4	[147]
Supramolecular ensemble 3:CuNPs	CuNPs: 3–20 nm	C-H alkynylation	60 W tungsten filament bulb	Room Temp.	DMSO, K_2CO_3	8 h	72%	-	[148]
Pd-Cu/SiC	Pd-Cu NPs: <5 nm	Sonogashira	300 W Xe lamp	60 °C	DMF, Cs_2CO_3	8 h	99%	-	[144]
CuPd@NH_2-UiO-66(Zr)	CuPd alloy nanoclusters: ~0.9 nm	Suzuki	300 W Xe lamp (420–800 nm)	Room Temp.	DMF/H_2O (1:1), TEA	4 h	99%	-	[145]
Cu/Cu_2O NPs	Tetrahexahedron: ~µm	Ullmann	Xe lamp	-	-	12 h	77%	-	[149]

Table 2. *Cont.*

Photocatalyst	Size and Shape	Reaction	Light Source	Reaction Temp.	Solvent, Base	Time	Yield	TOF (h^{-1})	Ref.
Pd hexagonal nanoplates	60.4 ± 19.3 nm (20.5 ± 3.7 nm thickness)	Suzuki	Xe lamp (300–1000 nm)	25 °C	EtOH, K_2CO_3	3 h	-	~288	[150]
Cu_7S_4@Pd	Cu_7S_4: 14 nm Pd: 4.3 nm	Suzuki	1500-nm diode laser	Room Temp.	H_2O, NaOH	0.5 h	97%	-	[151]
Pd/$WO_{3\text{-}x}$ NWs	Pd: ~5 nm $WO_{3\text{-}x}$ NWs: >µm (length), ~10 nm (diameter)	Suzuki	500 W Xe lamp (>650 nm)	-	EtOH, K_2CO_3	100 min	68.75%	-	[152]
Pd nanoflowers	150 nm	Suzuki	300 W Xe lamp (>475 nm)	Room Temp.	EtOH Cs_2CO_3	4 h	96%	-	[153]
Pd/TiO_2	-	Suzuki	15 W white LED	28 °C	H_2O-PEG, $NaOC(CH_3)_3$	4 h	93%	-	[154]
Pd/ZnO	~25 nm	Suzuki	11 W white LED lamp	Room Temp.	H_2O, Cs_2CO_3	40 min	>99%	-	[155]

4. Summary and Outlook

Herein, we reviewed the research and development of plasmonic hybrid nano-catalysts for two types of photocatalytic C–C coupling reactions: C–C coupling in CO_2 reduction to hydrocarbon fuels and C–C cross-coupling in organic chemistry. The C–C coupling in CO_2 reduction into multi-carbon fuels can be promoted with the aid of plasmonic NPs as both light absorbers and affinity sites for reactants. Likewise, Suzuki coupling can also be represented in C–C cross-coupling reactions, including Heck, Sonogashira, Stille, Negishi, and other reactions, typically using Pd as an active catalyst and plasmonic NPs with semiconductors as light-responsive materials to accelerate photocatalytic reactions. As mentioned above, the performances of the photocatalytic CO_2 reduction and C–C cross-coupling reactions are summarized in Tables 1 and 2.

Although plasmonic hybrid nano-catalysts for photocatalytic C–C cross-coupling in CO_2 reduction to hydrocarbon and C–C coupling in organic chemistry have been intensively investigated for their ability to contribute to the fine-chemical industry, energy sector, and environmental fields, and for solving challenges that still exist in synthesizing suitable photocatalysts by reaching high quantum yields for commercialization, controlling photothermal effects may affect reactions, and help understand the mechanism. As for C–C coupling in CO_2 reduction to value-added products, multi-carbon production is still much more difficult than C_1 production because of the requirement of multiple electrons, steps, and low selectivity. In addition, Cu has not been properly utilized as a plasmonic material that is cheaper than gold and silver. Thus, developing new hybrid materials with high efficiency could be one of the possible solutions. As for C–C cross-coupling in organic chemistry, the photocatalytic reaction, even Suzuki coupling, has no unified reaction system, where the efficiency varies widely depending on the reaction conditions, reactants, etc., and integrated mechanism. In addition, only a few studies on other photocatalytic C–C coupling reactions including Heck, Sonogashira, Stille, and Negishi coupling, except Suzuki coupling, have been conducted. Moreover, from an economic point of view, C–C cross-coupling reactions typically require expensive Pd active catalysts, which makes commercialization more difficult, so the Pd-free reaction needs to be actively studied.

Author Contributions: Conceptualization, D.-K.L. Investigation, H.H.S. Writing—Original Draft Preparation, H.H.S. Writing—Review and Editing, Y.D.S. and D.-K.L. Supervision, D.-K.L. Project Administration, Y.D.S. and D.-K.L. Funding Acquisition, Y.D.S. and D.-K.L. All authors have read and agreed to the published version of the manuscript.

Funding: This research is supported by the KRICT (KK2061-23), Bio Industrial Strategic Technology Development Program (No. 10077582) funded by the Ministry of Trade, Industry & Energy (MOTIE, Korea), and the Global Research Laboratory (GRL) Program of the National Research Foundation of Korea (NRF) funded by the Ministry of Science and ICT (No. 2016911815). This research is also supported by the National Research Foundation of Korea (2016R1A2B3013825, 2017M3D1A1039421, 2016M3A9B5940991) and the KU-KIST Research Fund.

Conflicts of Interest: The authors declare no conflict of interest.

References

1. Aman, M.M.; Solangi, K.H.; Hossain, M.S.; Badarudin, A.; Jasmon, G.B.; Mokhlis, H.; Bakar, A.H.A.; Kazi, S.N. A review of safety, health and environmental (SHE) issues of solar energy system. *Renew. Sustain. Energy Rev.* **2015**, *41*, 1190–1204. [CrossRef]
2. Hosenuzzaman, M.; Rahim, N.A.; Selvaraj, J.; Hasanuzzaman, M.; Malek, A.B.M.A.; Nahar, A. Global prospects, progress, policies, and environmental impact of solar photovoltaic power generation. *Renew. Sustain. Energy Rev.* **2015**, *41*, 284–297. [CrossRef]
3. Spasiano, D.; Marotta, R.; Malato, S.; Fernandez-Ibañez, P.; Di Somma, I. Solar photocatalysis: Materials, reactors, some commercial, and pre-industrialized applications. a comprehensive approach. *Appl. Catal. B* **2015**, *170*, 90–123. [CrossRef]
4. Long, R.; Li, Y.; Song, L.; Xiong, Y. Coupling solar energy into reactions: Materials design for surface plasmon-mediated catalysis. *Small* **2015**, *11*, 3873–3889. [CrossRef] [PubMed]
5. Smith, J.G.; Faucheaux, J.A.; Jain, P.K. Plasmon resonances for solar energy harvesting: A mechanistic outlook. *Nano Today* **2015**, *10*, 67–80. [CrossRef]
6. Goodenough, J.B. Energy storage materials: A perspective. *Energy Storage Mater.* **2015**, *1*, 158–161. [CrossRef]

7. Halabi, M.A.; Al-Qattan, A.; Al-Otaibi, A. Application of solar energy in the oil industry—Current status and future prospects. *Renew. Sustain. Energy Rev.* **2015**, *43*, 296–314. [CrossRef]
8. Alper, E.; Orhan, O.Y. CO_2 utilization: Developments in conversion processes. *Petroleum* **2017**, *3*, 109–126. [CrossRef]
9. Du, C.; Wang, X.; Chen, W.; Feng, S.; Wen, J.; Wu, Y.A. CO_2 transformation to multicarbon products by photocatalysis and electrocatalysis. *Mater. Today Adv.* **2020**, *6*, 100071. [CrossRef]
10. Royer, M.E. Réduction de l'acide carbonique en acide formique. *Comptes Rendus* **1870**, *1870*, 731–732.
11. Halmann, M. Photoelectrochemical reduction of aqueous carbon dioxide on p-type gallium phosphide in liquid junction solar cells. *Nature* **1978**, *275*, 115–116. [CrossRef]
12. Inoue, T.; Fujishima, A.; Konishi, S.; Honda, K. Photoelectrocatalytic reduction of carbon dioxide in aqueous suspensions of semiconductor powders. *Nature* **1979**, *277*, 637–638. [CrossRef]
13. Li, K.; Peng, B.; Peng, T. Recent advances in heterogeneous photocatalytic CO_2 conversion to solar fuels. *ACS Catal.* **2016**, *6*, 7485–7527. [CrossRef]
14. Wang, C.; Sun, Z.; Zheng, Y.; Hu, Y.H. Recent progress in visible light photocatalytic conversion of carbon dioxide. *J. Mater. Chem. A* **2019**, *7*, 865–887. [CrossRef]
15. Kim, D.; Sakimoto, K.K.; Hong, D.; Yang, P. Artificial photosynthesis for sustainable fuel and chemical production. *Angew. Chem. Int. Ed.* **2015**, *54*, 3259–3266. [CrossRef]
16. Marshall, J. Solar energy: Springtime for the artificial leaf. *Nature* **2014**, *510*, 22–24. [CrossRef] [PubMed]
17. Creel, E.B.; McCloskey, B.D. Scalable CO_2-to-oxygenate production. *Nat. Catal.* **2018**, *1*, 6–7. [CrossRef]
18. Bushuyev, O.S.; De Luna, P.; Dinh, C.T.; Tao, L.; Saur, G.; van de Lagemaat, J.; Kelley, S.O.; Sargent, E.H. What should we make with CO_2 and how can we make it? *Joule* **2018**, *2*, 825–832. [CrossRef]
19. Li, H.; Johansson Seechurn, C.C.C.; Colacot, T.J. Development of preformed Pd catalysts for cross-coupling reactions, beyond the 2010 Nobel prize. *ACS Catal.* **2012**, *2*, 1147–1164. [CrossRef]
20. Shi, W.; Liu, C.; Lei, A. Transition-metal catalyzed oxidative cross-coupling reactions to form C-C bonds involving organometallic reagents as nucleophiles. *Chem. Soc. Rev.* **2011**, *40*, 2761–2776. [CrossRef]
21. Miyaura, N.; Suzuki, A. Palladium-catalyzed cross-coupling reactions of organoboron compounds. *Chem. Rev.* **1995**, *95*, 2457–2483. [CrossRef]
22. Suzuki, A. Cross-coupling reactions of organoboranes: An easy way to construct C–C bonds (Nobel lecture). *Angew. Chem. Int. Ed.* **2011**, *50*, 6722–6737. [CrossRef] [PubMed]
23. Bariwal, J.; Van der Eycken, E. C–N bond forming cross-coupling reactions: An overview. *Chem. Soc. Rev.* **2013**, *42*, 9283–9303. [CrossRef]
24. Tamao, K.; Sumitani, K.; Kumada, M. Selective carbon–carbon bond formation by cross-coupling of grignard reagents with organic halides. catalysis by nickel-phosphine complexes. *J. Am. Chem. Soc.* **1972**, *94*, 4374–4376. [CrossRef]
25. Miyaura, N.; Yamada, K.; Suzuki, A. A new stereospecific cross-coupling by the palladium-catalyzed reaction of 1-alkenylboranes with 1-alkenyl or 1-alkynyl halides. *Tetrahedron Lett.* **1979**, *20*, 3437–3440. [CrossRef]
26. Heck, R.F.; Nolley, J.P., Jr. Palladium-catalyzed vinylic hydrogen substitution reactions with aryl, benzyl, and styryl halides. *J. Org. Chem.* **1972**, *37*, 2320–2322. [CrossRef]
27. Negishi, E.-I.; Baba, S. Novel stereoselective alkenyl–aryl coupling *via* nickel-catalysed reaction of alkenylanes with aryl halides. *J. Chem. Soc. Chem. Commun.* **1976**, 596b–597b. [CrossRef]
28. Ishiyama, T.; Matsuda, N.; Miyaura, N.; Suzuki, A. Platinum(0)-catalyzed diboration of alkynes. *J. Am. Chem. Soc.* **1993**, *115*, 11018–11019. [CrossRef]
29. Ishiyama, T.; Murata, M.; Miyaura, N. Palladium(0)-catalyzed cross-coupling reaction of alkoxydiboron with haloarenes: A direct procedure for arylboronic esters. *J. Org. Chem.* **1995**, *60*, 7508–7510. [CrossRef]
30. Guram, A.S.; Rennels, R.A.; Buchwald, S.L. A simple catalytic method for the conversion of aryl bromides to arylamines. *Angew. Chem. Int. Ed. Engl.* **1995**, *34*, 1348–1350. [CrossRef]
31. Louie, J.; Hartwig, J.F. Palladium-catalyzed synthesis of arylamines from aryl halides. Mechanistic studies lead to coupling in the absence of tin reagents. *Tetrahedron Lett.* **1995**, *36*, 3609–3612. [CrossRef]
32. Johansson Seechurn, C.C.C.; Kitching, M.O.; Colacot, T.J.; Snieckus, V. Palladium-catalyzed cross-coupling: A historical contextual perspective to the 2010 Nobel prize. *Angew. Chem. Int. Ed.* **2012**, *51*, 5062–5085. [CrossRef] [PubMed]
33. Diederich, F.; Stang, P.J. *Metal-Catalyzed Cross-Coupling Reactions*; Wiley-VCH: Weinheim, Germany, 2004.
34. Fihri, A.; Bouhrara, M.; Nekoueishahraki, B.; Basset, J.-M.; Polshettiwar, V. Nanocatalysts for Suzuki cross-coupling reactions. *Chem. Soc. Rev.* **2011**, *40*, 5181–5203. [CrossRef] [PubMed]
35. Biffis, A.; Centomo, P.; Del Zotto, A.; Zecca, M. Pd metal catalysts for cross-couplings and related reactions in the 21st century: A critical review. *Chem. Rev.* **2018**, *118*, 2249–2295. [CrossRef]
36. Linsebigler, A.L.; Lu, G.; Yates, J.T., Jr. Photocatalysis on TiO_2 surfaces: Principles, mechanisms, and selected results. *Chem. Rev.* **1995**, *95*, 735–758. [CrossRef]
37. Chen, X.; Mao, S.S. Titanium dioxide nanomaterials: Synthesis, properties, modifications, and applications. *Chem. Rev.* **2007**, *107*, 2891–2959. [CrossRef]
38. Zayat, M.; Garcia-Parejo, P.; Levy, D. Preventing UV-light damage of light sensitive materials using a highly protective UV-absorbing coating. *Chem. Soc. Rev.* **2007**, *36*, 1270–1281. [CrossRef]

39. Andrady, A.L.; Hamid, H.S.; Torikai, A. Effects of climate change and UV-B on materials. *Photochem. Photobiol. Sci.* **2003**, *2*, 68–72. [CrossRef]
40. Andrady, A.L.; Hamid, H.; Torikai, A. Effects of solar UV and climate change on materials. *Photochem. Photobiol. Sci.* **2011**, *10*, 292–300. [CrossRef]
41. Wang, C.; Astruc, D. Nanogold plasmonic photocatalysis for organic synthesis and clean energy conversion. *Chem. Soc. Rev.* **2014**, *43*, 7188–7216. [CrossRef]
42. Rycenga, M.; Cobley, C.M.; Zeng, J.; Li, W.; Moran, C.H.; Zhang, Q.; Qin, D.; Xia, Y. Controlling the synthesis and assembly of silver nanostructures for plasmonic applications. *Chem. Rev.* **2011**, *111*, 3669–3712. [CrossRef] [PubMed]
43. Sherry, L.J.; Chang, S.-H.; Schatz, G.C.; Van Duyne, R.P.; Wiley, B.J.; Xia, Y. Localized surface plasmon resonance spectroscopy of single silver nanocubes. *Nano Lett.* **2005**, *5*, 2034–2038. [CrossRef] [PubMed]
44. Zhang, Y.; He, S.; Guo, W.; Hu, Y.; Huang, J.; Mulcahy, J.R.; Wei, W.D. Surface-plasmon-driven hot electron photochemistry. *Chem. Rev.* **2018**, *118*, 2927–2954. [CrossRef] [PubMed]
45. Kale, M.J.; Avanesian, T.; Christopher, P. Direct photocatalysis by plasmonic nanostructures. *ACS Catal.* **2014**, *4*, 116–128. [CrossRef]
46. Chen, H.; Shao, L.; Li, Q.; Wang, J. Gold nanorods and their plasmonic properties. *Chem. Soc. Rev.* **2013**, *42*, 2679–2724. [CrossRef] [PubMed]
47. Nehl, C.L.; Hafner, J.H. Shape-dependent plasmon resonances of gold nanoparticles. *J. Mater. Chem.* **2008**, *18*, 2415–2419. [CrossRef]
48. Farokhnezhad, M.; Esmaeilzadeh, M.; Nourian, M.; Jalaeikhoo, H.; Rajaeinejad, M.; Iravani, S.; Majidzadeh-A, K. Silica–gold nanoshell@graphene: A novel class of plasmonic nanoagents for photothermal cancer therapy. *J. Phys. D Appl. Phys.* **2020**, *53*, 405401. [CrossRef]
49. Oldenburg, S.J.; Averitt, R.D.; Westcott, S.L.; Halas, N.J. Nanoengineering of optical resonances. *Chem. Phys. Lett.* **1998**, *288*, 243–247. [CrossRef]
50. Chen, J.; Saeki, F.; Wiley, B.J.; Cang, H.; Cobb, M.J.; Li, Z.-Y.; Au, L.; Zhang, H.; Kimmey, M.B.; Li, X.; et al. Gold nanocages: Bioconjugation and their potential use as optical imaging contrast agents. *Nano Lett.* **2005**, *5*, 473–477. [CrossRef]
51. Brongersma, M.L.; Halas, N.J.; Nordlander, P. Plasmon-induced hot carrier science and technology. *Nat. Nanotechnol.* **2015**, *10*, 25–34. [CrossRef]
52. Clavero, C. Plasmon-induced hot-electron generation at nanoparticle/metal-oxide interfaces for photovoltaic and photocatalytic devices. *Nat. Photonics* **2014**, *8*, 95–103. [CrossRef]
53. Vitousek, P.M.; Mooney, H.A.; Lubchenco, J.; Melillo, J.M. Human domination of Earth's ecosystems. *Science* **1997**, *277*, 494–499. [CrossRef]
54. Lewis, N.S.; Nocera, D.G. Powering the planet: Chemical challenges in solar energy utilization. *Proc. Natl. Acad. Sci. USA* **2006**, *103*, 15729–15735. [CrossRef] [PubMed]
55. Wang, W.-H.; Himeda, Y.; Muckerman, J.T.; Manbeck, G.F.; Fujita, E. CO_2 hydrogenation to formate and methanol as an alternative to photo- and electrochemical CO_2 reduction. *Chem. Rev.* **2015**, *115*, 12936–12973. [CrossRef]
56. Nielsen, C.J.; Herrmann, H.; Weller, C. Atmospheric chemistry and environmental impact of the use of amines in carbon capture and storage (CCS). *Chem. Soc. Rev.* **2012**, *41*, 6684–6704. [CrossRef]
57. Wu, J.; Huang, Y.; Ye, W.; Li, Y. CO_2 reduction: From the electrochemical to photochemical approach. *Adv. Sci.* **2017**, *4*, 1700194. [CrossRef]
58. Dahl, S.; Chorkendorff, I. Towards practical implementation. *Nat. Mater.* **2012**, *11*, 100–101. [CrossRef]
59. Schneider, J.; Jia, H.; Muckerman, J.T.; Fujita, E. Thermodynamics and kinetics of CO_2, CO, and H^+ binding to the metal centre of CO_2 reduction catalysts. *Chem. Soc. Rev.* **2012**, *41*, 2036–2051. [CrossRef]
60. Hu, B.; Guild, C.; Suib, S.L. Thermal, electrochemical, and photochemical conversion of CO_2 to fuels and value-added products. *J. CO_2 Util.* **2013**, *1*, 18–27. [CrossRef]
61. Li, X.; Wen, J.; Low, J.; Fang, Y.; Yu, J. Design and fabrication of semiconductor photocatalyst for photocatalytic reduction of CO_2 to solar fuel. *Sci. China Mater.* **2014**, *57*, 70–100. [CrossRef]
62. Gao, D.; Arán-Ais, R.M.; Jeon, H.S.; Cuenya, B.R. Rational catalyst and electrolyte design for CO_2 electroreduction towards multicarbon products. *Nat. Catal.* **2019**, *2*, 198–210. [CrossRef]
63. Hepburn, C.; Adlen, E.; Beddington, J.; Carter, E.A.; Fuss, S.; Mac Dowell, N.; Minx, J.C.; Smith, P.; Williams, C.K. The technological and economic prospects for CO_2 utilization and removal. *Nature* **2019**, *575*, 87–97. [CrossRef] [PubMed]
64. Morris, A.J.; Meyer, G.J.; Fujita, E. Molecular approaches to the photocatalytic reduction of carbon dioxide for solar fuels. *Acc. Chem. Res.* **2009**, *42*, 1983–1994. [CrossRef] [PubMed]
65. Kiesgen de_Richter, R.; Ming, T.; Caillol, S. Fighting global warming by photocatalytic reduction of CO_2 using giant photocatalytic reactors. *Renew. Sustain. Energy Rev.* **2013**, *19*, 82–106. [CrossRef]
66. Marszewski, M.; Cao, S.; Yu, J.; Jaroniec, M. Semiconductor-based photocatalytic CO_2 conversion. *Mater. Horiz.* **2015**, *2*, 261–278. [CrossRef]
67. Razzaq, A.; In, S.-I. TiO_2 based nanostructures for photocatalytic CO_2 conversion to valuable chemicals. *Micromachines* **2019**, *10*, 326. [CrossRef]

68. Nguyen, T.P.; Nguyen, D.L.T.; Nguyen, V.-H.; Le, T.-H.; Vo, D.-V.N.; Trinh, Q.T.; Bae, S.-R.; Chae, S.Y.; Kim, S.Y.; Le, Q.V. Recent advances in TiO_2-based photocatalysts for reduction of CO_2 to fuels. *Nanomaterials* **2020**, *10*, 337. [CrossRef]
69. Kumar, D.; Lee, A.; Lee, T.; Lim, M.; Lim, D.-K. Ultrafast and efficient transport of hot plasmonic electrons by graphene for Pt Free, highly efficient visible-light responsive photocatalyst. *Nano Lett.* **2016**, *16*, 1760–1767. [CrossRef]
70. Yu, S.; Wilson, A.J.; Kumari, G.; Zhang, X.; Jain, P.K. Opportunities and challenges of solar-energy-driven carbon dioxide to fuel conversion with plasmonic catalysts. *ACS Energy Lett.* **2017**, *2*, 2058–2070. [CrossRef]
71. Liu, E.; Hu, Y.; Li, H.; Tang, C.; Hu, X.; Fan, J.; Chen, Y.; Bian, J. Photoconversion of CO_2 to methanol over plasmonic Ag/TiO_2 nano-wire films enhanced by overlapped visible-light-harvesting nanostructures. *Ceram. Int.* **2015**, *41*, 1049–1057. [CrossRef]
72. Louis, C.; Pluchery, O. *Gold Nanoparticles for Physics, Chemistry, and Biology*; Imperial College Press: London, UK, 2012.
73. Sarina, S.; Waclawik, E.R.; Zhu, H. Photocatalysis on supported gold and silver nanoparticles under ultraviolet and visible light irradiation. *Green Chem.* **2013**, *15*, 1814–1833. [CrossRef]
74. Cao, L.; Sahu, S.; Anilkumar, P.; Bunker, C.E.; Xu, J.; Fernando, K.A.S.; Wang, P.; Guliants, E.A.; Tackett, K.N.; Sun, Y.-P. Carbon nanoparticles as visible-light photocatalysts for efficient CO_2 conversion and beyond. *J. Am. Chem. Soc.* **2011**, *133*, 4754–4757. [CrossRef] [PubMed]
75. Hoffmann, M.R.; Moss, J.A.; Baum, M.M. Artificial photosynthesis: Semiconductor photocatalytic fixation of CO_2 to afford higher organic compounds. *Dalton Trans.* **2011**, *40*, 5151–5158. [CrossRef] [PubMed]
76. Tu, W.; Zhou, Y.; Li, H.; Li, P.; Zou, Z. Au@TiO_2 yolk–shell hollow spheres for plasmon-induced photocatalytic reduction of CO_2 to solar fuel *via* a local electromagnetic field. *Nanoscale* **2015**, *7*, 14232–14236. [CrossRef] [PubMed]
77. Yu, S.; Wilson, A.J.; Heo, J.; Jain, P.K. Plasmonic control of multi-electron transfer and C-C coupling in visible-light-driven CO_2 reduction on Au nanoparticles. *Nano Lett.* **2018**, *18*, 2189–2194. [CrossRef]
78. Zhao, J.; Liu, B.; Meng, L.; He, S.; Yuan, R.; Hou, Y.; Ding, Z.; Lin, H.; Zhang, Z.; Wang, X.; et al. Plasmonic control of solar-driven CO_2 conversion at the metal/ZnO interfaces. *Appl. Catal. B* **2019**, *256*, 117823. [CrossRef]
79. Becerra, J.; Nguyen, D.-T.; Gopalakrishnan, V.-N.; Do, T.-O. Plasmonic Au nanoparticles incorporated in the zeolitic imidazolate framework (ZIF-67) for the efficient sunlight-driven photoreduction of CO_2. *ACS Appl. Energy Mater.* **2020**, *3*, 7659–7665. [CrossRef]
80. Linic, S.; Christopher, P.; Ingram, D.B. Plasmonic-metal nanostructures for efficient conversion of solar to chemical energy. *Nat. Mater.* **2011**, *10*, 911–921. [CrossRef]
81. Cai, B.; Wang, J.; Han, D.; Gan, S.; Zhang, Q.; Wu, Z.; Niu, L. Ternary alloyed $AgCl_xBr_{1-x}$ nanocrystals: Facile modulation of electronic structures toward advanced photocatalytic performance. *Nanoscale* **2013**, *5*, 10989–10995. [CrossRef]
82. Cai, B.; Wang, J.; Gan, S.; Han, D.; Wu, Z.; Niu, L. A distinctive red Ag/AgCl photocatalyst with efficient photocatalytic oxidative and reductive activities. *J. Mater. Chem. A* **2014**, *2*, 5280–5286. [CrossRef]
83. Li, N.; Jiang, R.; Li, Y.; Zhou, J.; Ma, Q.; Shen, S.; Liu, M. Plasma-assisted photocatalysis of CH_4 and CO_2 into ethylene. *ACS Sustain. Chem. Eng.* **2019**, *7*, 11455–11463. [CrossRef]
84. Varghese, O.K.; Paulose, M.; LaTempa, T.J.; Grimes, C.A. High-rate solar photocatalytic conversion of CO_2 and water vapor to hydrocarbon fuels. *Nano Lett.* **2009**, *9*, 731–737. [CrossRef] [PubMed]
85. Tseng, I.-H.; Wu, J.C.-S. Chemical states of metal-loaded titania in the photoreduction of CO_2. *Catal. Today* **2004**, *97*, 113–119. [CrossRef]
86. Lee, S.; Kim, D.; Lee, J. Electrocatalytic production of C_3-C_4 compounds by conversion of CO_2 on a chloride-induced Bi-phasic Cu_2O-Cu catalyst. *Angew. Chem.* **2015**, *127*, 14914–14918. [CrossRef]
87. Rawat, K.S.; Mahata, A.; Pathak, B. Thermochemical and electrochemical CO_2 reduction on octahedral Cu nanocluster: Role of solvent towards product selectivity. *J. Catal.* **2017**, *349*, 118–127. [CrossRef]
88. Shown, I.; Hsu, H.-C.; Chang, Y.-C.; Lin, C.-H.; Roy, P.K.; Ganguly, A.; Wang, C.-H.; Chang, J.-K.; Wu, C.-I.; Chen, L.-C.; et al. Highly efficient visible light photocatalytic reduction of CO_2 to hydrocarbon fuels by Cu nanoparticle decorated graphene oxide. *Nano Lett.* **2014**, *14*, 6097–6103. [CrossRef]
89. Park, H.; Ou, H.-H.; Colussi, A.J.; Hoffmann, M.R. Artificial photosynthesis of C1–C3 hydrocarbons from water and CO_2 on titanate nanotubes decorated with nanoparticle elemental copper and CdS quantum dots. *J. Phys. Chem. A* **2015**, *119*, 4658–4666. [CrossRef]
90. Chen, Y.; Wang, M.; Ma, Y.; Li, Y.; Cai, J.; Li, Z. Coupling photocatalytic CO_2 reduction with benzyl alcohol oxidation to produce benzyl acetate over Cu_2O/Cu. *Catal. Sci. Technol.* **2018**, *8*, 2218–2223. [CrossRef]
91. Maluenda, I.; Navarro, O. Recent developments in the Suzuki–Miyaura reaction: 2010–2014. *Molecules* **2015**, *20*, 7528–7557. [CrossRef]
92. Teranishi, T.; Eguchi, M.; Kanehara, M.; Gwo, S. Controlled localized surface plasmon resonance wavelength for conductive nanoparticles over the ultraviolet to near-infrared region. *J. Mater. Chem.* **2011**, *21*, 10238–10242. [CrossRef]
93. Zielińska-Jurek, A. Progress, challenge, and perspective of bimetallic TiO_2-based photocatalysts. *J. Nanomater.* **2014**, *2014*, 208920. [CrossRef]
94. Wali, L.A.; Alwan, A.M.; Dheyab, A.B.; Hashim, D.A. Excellent fabrication of Pd-Ag NPs/PSi photocatalyst based on bimetallic nanoparticles for improving methylene blue photocatalytic degradation. *Optik* **2019**, *179*, 708–717. [CrossRef]
95. Lee, S.; Wy, Y.; Lee, Y.W.; Ham, K.; Han, S.W. Core–shell nanoparticle clusters enable synergistic integration of plasmonic and catalytic functions in a single platform. *Small* **2017**, *13*, 1701633. [CrossRef]

96. Furube, A.; Hashimoto, S. Insight into plasmonic hot-electron transfer and plasmon molecular drive: New dimensions in energy conversion and nanofabrication. *NPG Asia Mater.* **2017**, *9*, e454. [CrossRef]
97. Shan, H.; Yu, Y.; Wang, X.; Luo, Y.; Zu, S.; Du, B.; Han, T.; Li, B.; Li, Y.; Wu, J.; et al. Direct observation of ultrafast plasmonic hot electron transfer in the strong coupling regime. *Light Sci. Appl.* **2019**, *8*, 9. [CrossRef]
98. Huang, X.; Li, Y.; Chen, Y.; Zhou, H.; Duan, X.; Huang, Y. Plasmonic and catalytic AuPd nanowheels for the efficient conversion of light Into chemical energy. *Angew. Chem. Int. Ed.* **2013**, *52*, 6063–6067. [CrossRef]
99. Gangishetty, M.K.; Fontes, A.M.; Malta, M.; Kelly, T.L.; Scott, R.W.J. Improving the rates of Pd-catalyzed reactions by exciting the surface plasmons of AuPd bimetallic nanotriangles. *RSC Adv.* **2017**, *7*, 40218–40226. [CrossRef]
100. Sarina, S.; Zhu, H.; Jaatinen, E.; Xiao, Q.; Liu, H.; Jia, J.; Chen, C.; Zhao, J. Enhancing catalytic performance of palladium in gold and palladium alloy nanoparticles for organic synthesis reactions through visible light irradiation at ambient temperatures. *J. Am. Chem. Soc.* **2013**, *135*, 5793–5801. [CrossRef]
101. Xiao, Q.; Sarina, S.; Jaatinen, E.; Jia, J.; Arnold, D.P.; Liu, H.; Zhu, H. Efficient photocatalytic Suzuki cross-coupling reactions on Au-Pd alloy nanoparticles under visible light irradiation. *Green Chem.* **2014**, *16*, 4272–4285. [CrossRef]
102. Xiao, Q.; Sarina, S.; Bo, A.; Jia, J.; Liu, H.; Arnold, D.P.; Huang, Y.; Wu, H.; Zhu, H. Visible light-driven cross-coupling reactions at lower temperatures using a photocatalyst of palladium and gold alloy nanoparticles. *ACS Catal.* **2014**, *4*, 1725–1734. [CrossRef]
103. Sarina, S.; Jaatinen, E.; Xiao, Q.; Huang, Y.M.; Christopher, P.; Zhao, J.C.; Zhu, H.Y. Photon energy threshold in direct photocatalysis with metal nanoparticles: Key evidence from the action spectrum of the reaction. *J. Phys. Chem. Lett.* **2017**, *8*, 2526–2534. [CrossRef]
104. Zhang, S.; Chang, C.; Huang, Z.; Ma, Y.; Gao, W.; Li, J.; Qu, Y. Visible-light-activated Suzuki–Miyaura coupling reactions of aryl chlorides over the multifunctional Pd/Au/porous nanorods of CeO_2 catalysts. *ACS Catal.* **2015**, *5*, 6481–6488. [CrossRef]
105. Movahed, S.K.; Miraghaee, S.; Dabiri, M. AuPd alloy nanoparticles decorated graphitic carbon nitride as an excellent photocatalyst for the visible-light-enhanced Suzuki–Miyaura cross-coupling reaction. *J. Alloys Compd.* **2020**, *819*, 152994. [CrossRef]
106. Subudhi, S.; Mansingh, S.; Tripathy, S.P.; Mohanty, A.; Mohapatra, P.; Rath, D.; Parida, K. The fabrication of Au/Pd plasmonic alloys on UiO-66-NH_2: An efficient visible light-induced photocatalyst towards the Suzuki–Miyaura coupling reaction under ambient conditions. *Catal. Sci. Technol.* **2019**, *9*, 6585–6597. [CrossRef]
107. Kataria, M.; Kumar, M.; Singh, Z.; Bhalla, V. Gold nanoparticles immobilized polymeric PBI derivative: Productive, portable, and photocatalytic system for Heck coupling. *ACS Sustain. Chem. Eng.* **2018**, *6*, 8223–8229. [CrossRef]
108. Nemygina, N.A.; Nikoshvili, L.Z.; Tiamina, I.Y.; Bykov, A.V.; Smirnov, I.S.; LaGrange, T.; Kaszkur, Z.; Matveeva, V.G.; Sulman, E.M.; Kiwi-Minsker, L. Au core–Pd shell bimetallic nanoparticlesi within hyper-cross-linked polystyrene for mechanistic study of Suzuki cross-coupling: Homogeneous or heterogeneous catalysis? *Org. Process Res. Dev.* **2018**, *22*, 1606–1613. [CrossRef]
109. Han, D.; Bao, Z.; Xing, H.; Yang, Y.; Ren, Q.; Zhang, Z. Fabrication of plasmonic Au-Pd alloy nanoparticles for photocatalytic Suzuki–Miyaura reactions under ambient conditions. *Nanoscale* **2017**, *9*, 6026–6032. [CrossRef]
110. Tyagi, A.; Yamamoto, A.; Yoshida, H. Photocatalytic Ullmann coupling of aryl halides by a novel blended catalyst consisting of a TiO_2 photocatalyst and an Al_2O_3 supported Pd-Au bimetallic catalyst. *Catal. Sci. Technol.* **2018**, *8*, 6196–6203. [CrossRef]
111. Tyagi, A.; Yamamoto, A.; Yoshida, H. Novel blended catalysts consisting of a TiO_2 photocatalyst and an Al_2O_3 supported Pd-Au bimetallic catalyst for direct dehydrogenative cross-coupling between arenes and tetrahydrofuran. *RSC Adv.* **2018**, *8*, 24021–24028. [CrossRef]
112. Rohani, S.; Ziarati, A.; Ziarani, G.M.; Badiei, A.; Burgi, T. Engineering of highly active Au/Pd supported on hydrogenated urchin-like yolk@shell TiO_2 for visible light photocatalytic Suzuki coupling. *Catal. Sci. Technol.* **2019**, *9*, 3820–3827. [CrossRef]
113. Verma, P.; Kuwahara, Y.; Mori, K.; Yamashita, H. Pd/Ag and Pd/Au bimetallic nanocatalysts on mesoporous silica for plasmon-mediated enhanced catalytic activity under visible light irradiation. *J. Mater. Chem. A* **2016**, *4*, 10142–10150. [CrossRef]
114. Li, X.-H.; Baar, M.; Blechert, S.; Antonietti, M. Facilitating room-temperature Suzuki coupling reaction with light: Mott-Schottky photocatalyst for C-C coupling. *Sci. Rep.* **2013**, *3*, 1743. [CrossRef]
115. Shin, H.H.; Kang, E.; Park, H.; Han, T.; Lee, C.-H.; Lim, D.-K. Pd-nanodot decorated MoS_2 nanosheets as a highly efficient photocatalyst for the visible-light-induced Suzuki–Miyaura coupling reaction. *J. Mater. Chem. A* **2017**, *5*, 24965–24971. [CrossRef]
116. Raza, F.; Yim, D.; Park, J.H.; Kim, H.-I.; Jeon, S.-J.; Kim, J.-H. Structuring Pd nanoparticles on 2H-WS_2 nanosheets induces excellent photocatalytic activity for cross-coupling reactions under visible light. *J. Am. Chem. Soc.* **2017**, *139*, 14767–14774. [CrossRef]
117. Chen, J.-H.; Jang, C.; Xiao, S.; Ishigami, M.; Fuhrer, M.S. Intrinsic and extrinsic performance limits of graphene devices on SiO_2. *Nat. Nanotechnol.* **2008**, *3*, 206–209. [CrossRef]
118. Xiang, Q.; Yu, J.; Jaroniec, M. Graphene-based semiconductor photocatalysts. *Chem. Soc. Rev.* **2012**, *41*, 782–796. [CrossRef]
119. Kang, E.; Shin, H.H.; Lim, D.-K. Interface-controlled Pd nanodot-Au nanoparticle colloids for efficient visible-light-induced photocatalytic Suzuki–Miyaura coupling reaction. *Catalysts* **2018**, *8*, 463. [CrossRef]
120. Sahoo, M.; Mansingh, S.; Subudhi, S.; Mohapatra, P.; Parida, K. A plasmonic AuPd bimetallic nanoalloy decorated over a GO/LDH hybrid nanocomposite *via* a green synthesis route for robust Suzuki coupling reactions: A paradigm shift towards a sustainable future. *Catal. Sci. Technol.* **2019**, *9*, 4678–4692. [CrossRef]
121. Shin, H.H.; Han, T.; Yang, W.; Lim, D.-K. Pd^{2+}-conjugated reduced graphene oxide as a highly efficient visible-light-induced photocatalytic Suzuki–Miyaura coupling. *Carbon* **2019**, *143*, 362–370. [CrossRef]
122. Wang, L.; Xu, X.; Cheng, Q.; Dou, S.X.; Du, Y. Near-infrared-driven photocatalysts: Design, construction, and applications. *Small* **2019**, 1904107. [CrossRef]

123. Murphy, C.J.; Sau, T.K.; Gole, A.M.; Orendorff, C.J.; Gao, J.; Gou, L.; Hunyadi, S.E.; Li, T. Anisotropic metal nanoparticles: Synthesis, assembly, and optical applications. *J. Phys. Chem. B* **2005**, *109*, 13857–13870. [CrossRef]
124. Khlebtsov, B.N.; Khlebtsov, N.G. Multipole plasmons in metal nanorods: Scaling properties and dependence on particle size, shape, orientation, and dielectric environment. *J. Phys. Chem. C* **2007**, *111*, 11516–11527. [CrossRef]
125. Encina, E.R.; Coronado, E.A. Resonance conditions for multipole plasmon excitations in noble metal nanorods. *J. Phys. Chem. C* **2007**, *111*, 16796–16801. [CrossRef]
126. Wang, J.-H.; Chen, M.; Luo, Z.-J.; Ma, L.; Zhang, Y.-F.; Chen, K.; Zhou, L.; Wang, Q.-Q. Ceria-coated gold nanorods for plasmon-enhanced near-infrared photocatalytic and photoelectrochemical performances. *J. Phys. Chem. C* **2016**, *120*, 14805–14812. [CrossRef]
127. Wang, F.; Li, C.; Chen, H.; Jiang, R.; Sun, L.-D.; Li, Q.; Wang, J.; Yu, J.C.; Yan, C.-H. Plasmonic harvesting of light energy for Suzuki coupling reactions. *J. Am. Chem. Soc.* **2013**, *135*, 5588–5601. [CrossRef]
128. Wen, M.; Takakura, S.; Fuku, K.; Mori, K.; Yamashita, H. Enhancement of Pd-catalyzed Suzuki–Miyaura coupling reaction assisted by localized surface plasmon resonance of Au nanorods. *Catal. Today* **2015**, *242*, 381–385. [CrossRef]
129. Guo, J.; Zhang, Y.; Shi, L.; Zhu, Y.; Mideksa, M.F.; Hou, K.; Zhao, W.; Wang, D.; Zhao, M.; Zhang, X.; et al. Boosting hot electrons in hetero-superstructures for plasmon-enhanced catalysis. *J. Am. Chem. Soc.* **2017**, *139*, 17964–17972. [CrossRef]
130. Verkaaik, M.; Grote, R.; Meulendijks, N.; Sastre, F.; Weckhuysen, B.M.; Buskens, P. Suzuki-Miyaura cross-coupling using plasmonic Pd-decorated Au nanorods as catalyst: A study on the contribution of laser illumination. *ChemCatChem* **2019**, *11*, 4974–4980. [CrossRef]
131. Yoshii, T.; Kuwahara, Y.; Mori, K.; Yamashita, H. Design of Pd–graphene–Au nanorod nanocomposite catalyst for boosting Suzuki–Miyaura coupling reaction by assistance of surface plasmon resonance. *J. Phys. Chem. C* **2019**, *123*, 24575–24583. [CrossRef]
132. Gao, S.; Shang, N.; Feng, C.; Wang, C.; Wang, Z. Graphene oxide–palladium modified Ag-AgBr: A visible-light-responsive photocatalyst for the Suzuki coupling reaction. *RSC Adv.* **2014**, *4*, 39242–39247. [CrossRef]
133. Verma, P.; Kuwahara, Y.; Mori, K.; Yamashita, H. Synthesis and characterization of a Pd/Ag bimetallic nanocatalyst on SBA-15 mesoporous silica as a plasmonic catalyst. *J. Mater. Chem. A* **2015**, *3*, 18889–18897. [CrossRef]
134. Sharma, K.; Kumar, M.; Bhalla, V. Aggregates of the pentacenequinone derivative as reactors for the preparation of Ag@Cu_2O core-shell NPs: An active photocatalyst for Suzuki and Suzuki type coupling reactions. *Chem. Commun.* **2015**, *51*, 12529–12532. [CrossRef] [PubMed]
135. Chopra, R.; Kumar, M.; Bhalla, V. Development of a supramolecular ensemble of an AIEE active hexaphenylbenzene derivative and Ag@Cu_2O Ccore-shell NPs: An efficient photocatalytic system for C-H activation. *Chem. Commun.* **2016**, *52*, 10179–10182. [CrossRef]
136. Chen, Y.; Feng, L. Silver nanoparticles doped TiO_2 catalyzed Suzuki coupling of bromoaryl with phenylboronic acid under visible light. *J. Photochem. Photobiol. B* **2020**, *205*, 111807. [CrossRef] [PubMed]
137. Chan, G.H.; Zhao, J.; Hicks, E.M.; Schatz, G.C.; Van Duyne, R.P. Plasmonic properties of copper nanoparticles fabricated by nanosphere lithography. *Nano Lett.* **2007**, *7*, 1947–1952. [CrossRef]
138. Liu, P.; Wang, H.; Li, X.; Rui, M.; Zeng, H. Localized surface plasmon resonance of Cu nanoparticles by laser ablation in liquid media. *RSC Adv.* **2015**, *5*, 79738–79745. [CrossRef]
139. Gezgin, S.Y.; Kepceoğlu, A.; Kılıç, H.Ş. An experimental investigation of localised surface plasmon resonance (LSPR) for Cu nanoparticles depending as a function of laser pulse number in pulsed laser deposition. *AIP Conf. Proc.* **2017**, *1815*, 030020.
140. Kim, J.H.; Ehrman, S.H.; Germer, T.A. Influence of particle oxide coating on light scattering by submicron metal particles on silicon wafers. *Appl. Phys. Lett.* **2004**, *84*, 1278–1280. [CrossRef]
141. DeSario, P.A.; Pietron, J.J.; Brintlinger, T.H.; McEntee, M.; Parker, J.F.; Baturina, O.; Stroud, R.M.; Rolison, D.R. Oxidation-stable plasmonic copper nanoparticles in photocatalytic TiO_2 nanoarchitectures. *Nanoscale* **2017**, *9*, 11720–11729. [CrossRef]
142. Huang, Y.; Liu, Z.; Gao, G.; Xiao, G.; Du, A.; Bottle, S.; Sarina, S.; Zhu, H. Stable copper nanoparticle photocatalysts for selective epoxidation of alkenes with visible light. *ACS Catal.* **2017**, *7*, 4975–4985. [CrossRef]
143. Zhang, P.; Song, T.; Wang, T.; Zeng, H. Plasmonic Cu nanoparticle on reduced graphene oxide nanosheet support: An efficient photocatalyst for improvement of near-infrared photocatalytic H_2 evolution. *Appl. Catal. B* **2018**, *225*, 172–179. [CrossRef]
144. Wang, B.; Wang, Y.; Li, J.; Guo, X.; Bai, G.; Tong, X.; Jin, G.; Guo, X. Photocatalytic Sonogashira reaction over silicon carbide supported Pd-Cu alloy nanoparticles under visible light irradiation. *Catal. Sci. Technol.* **2018**, *8*, 3357–3362. [CrossRef]
145. Sun, D.; Xu, M.; Jiang, Y.; Long, J.; Li, Z. Small-sized bimetallic CuPd nanoclusters encapsulated inside cavity of NH_2-UiO-66(Zr) with superior performance for light-induced Suzuki coupling reaction. *Small Methods* **2018**, *2*, 1800164. [CrossRef]
146. Guo, X.; Hao, C.; Jin, G.; Zhu, H.-Y.; Guo, X.-Y. Copper nanoparticles on graphene support: An efficient photocatalyst for coupling of nitroaromatics in visible light. *Angew. Chem. Int. Ed.* **2014**, *53*, 1973–1977. [CrossRef] [PubMed]
147. Cui, Y.-L.; Guo, X.-N.; Wang, Y.-Y.; Guo, X.-Y. Visible-light-driven photocatalytic N-arylation of imidazole derivatives and arylboronic acids on Cu/graphene catalyst. *Sci. Rep.* **2015**, *5*, 12005. [CrossRef]
148. Kaur, S.; Kumar, M.; Bhalla, V. Supramolecular ensemble of PBI derivative and copper nanoparticles: A light harvesting antenna for photocatalytic C(sp^2)–H functionalization. *Green Chem.* **2016**, *18*, 5870–5883. [CrossRef]
149. Li, M.; Xing, X.; Ma, Z.; Lv, J.; Fu, P.; Li, Z. Synthesis of composition tunable and (111)-faceted Cu/Cu_2O nanoparticles toward photocatalytic, ligand-free, and solvent-free C-N Ullmann coupling reactions. *ACS Sustain. Chem. Eng.* **2018**, *6*, 5495–5503. [CrossRef]

150. Trinh, T.T.; Sato, R.; Sakamoto, M.; Fujiyoshi, Y.; Haruta, M.; Kurata, H.; Teranishi, T. Visible to near-infrared plasmon-enhanced catalytic activity of Pd hexagonal nanoplates for the Suzuki coupling reaction. *Nanoscale* **2015**, *7*, 12435–12444. [CrossRef]
151. Cui, J.; Li, Y.; Liu, L.; Chen, L.; Xu, J.; Ma, J.; Fang, G.; Zhu, E.; Wu, H.; Zhao, L.; et al. Near-infrared plasmonic-enhanced solar energy harvest for highly efficient photocatalytic reactions. *Nano Lett.* **2015**, *15*, 6295–6301. [CrossRef]
152. Lou, Z.; Gu, Q.; Liao, Y.; Yu, S.; Xue, C. Promoting Pd-catalyzed Suzuki coupling reactions through near-infrared plasmon excitation of WO_{3-x} nanowires. *Appl. Catal. B* **2016**, *184*, 258–263. [CrossRef]
153. Sarhid, I.; Abdellah, I.; Martini, C.; Huc, V.; Dragoe, D.; Beaunier, P.; Lampre, I.; Remita, H. Plasmonic catalysis for the Suzuki–Miyaura cross-coupling reaction using palladium nanoflowers. *New J. Chem.* **2019**, *43*, 4349–4355. [CrossRef]
154. Koohgard, M.; Hosseini-Sarvari, M. Enhancement of Suzuki–Miyaura coupling reaction by photocatalytic palladium nanoparticles anchored to TiO_2 under visible light irradiation. *Catal. Commun.* **2018**, *111*, 10–15. [CrossRef]
155. Hosseini-Sarvari, M.; Bazyar, Z. Visible light driven photocatalytic cross-coupling reactions on nano Pd/ZnO photocatalyst at room-temperature. *ChemistrySelect* **2018**, *3*, 1898–1907. [CrossRef]